



# Two Aluminium Mixtures for In-stream Phosphorus Adsorption to Reduce External Loads

MSc Thesis AEW; 2023 M79  
Johan van Snippenberg



# Two Aluminium Mixtures for In-Stream Phosphorus Adsorption to Reduce Diffuse External Loads

2023 M79

Johan Christiaan van Snippenberg  
1164090

## **Study Programme**

MEE - MSc Earth and Environment  
Specialisation C - Biology and Chemistry of Soil and Water  
AEW-80436

## **Chair Group**

Aquatic Ecology and Water Quality Management

## **Supervisors**

Dr. ir. M.F.L.L.W. Lürling  
Dr. M.N.T. Mucci

## **Date**

February 14, 2024  
Wageningen University, Wageningen



## Abstract

Anthropogenic eutrophication and associated harmful algal blooms (HAB) are well-known threats to aquatic ecosystems in the 21<sup>st</sup> century. Watershed-wide diffuse nutrient sources are the most difficult to manage nutrient loads into aquatic ecosystems. Phosflow™ and EutroSORB® F are claimed to be able to remove P from flowing waters like agricultural ditches or tile-drainage outlets. To test whether they are fit for purpose, shaking, adsorption kinetics, batch adsorption, and fixed-bed adsorption experiments were carried out, along with other material characteristic tests: X-ray diffraction (XRD), aqua regia destruction and elemental analysis, and sequential P extraction. EutroSORB® F contains 40% böhmite ( $\gamma$ -AlOOH) and 41% calcite ( $\text{CaCO}_3$ ) by mass, separated over two size-modes. Phosflow™ contains 71% böhmite by mass and around  $4.3 \text{ mg Mg g}^{-1}$ . Both should be physically stable when in water with flow rates up to between  $2$  and  $2.8 \text{ L min}^{-1}$ , though EutroSORB® F is less sensitive to erosion than Phosflow™. Their equilibrium maximum adsorption capacities (MAC) are around  $10.3 \text{ mg P g}^{-1}$ , though P has greater affinity for EutroSORB® F than Phosflow™, with  $K$ -values of  $53$  and  $13 \text{ L g}^{-1}$  respectively. Fixed-bed MACs are around  $4.8$  and  $2.6 \text{ mg P g}^{-1}$  for EutroSORB® F than Phosflow™ respectively, but these are reduced to  $2.19$  and  $2.12 \text{ mg P g}^{-1}$  when using lake-water-based influent. P-fractionation indicates that böhmite plays an important role in P-sorption in both product, with precipitation of Ca-phosphate minerals possibly being prevalent in EutroSORB® F. It is recommended to test both products in larger-scale fixed-bed adsorption experiments under varying conditions regarding organic matter (OM), dissolved OM, and pH.



# Contents

<b>Abstract</b>	<b>iii</b>
<b>1 Introduction</b>	<b>1</b>
1.1 Eutrophication . . . . .	1
1.2 Mitigation, prevention, & restoration . . . . .	1
1.3 In-stream phosphorus adsorption . . . . .	2
<b>2 Methods &amp; Materials</b>	<b>3</b>
2.1 Size distributions, LOD, & LOI . . . . .	5
2.2 Aqua regia extraction & X-ray diffraction . . . . .	5
2.3 Shaking test . . . . .	6
2.4 Adsorption kinetics . . . . .	6
2.5 Adsorption isotherms . . . . .	7
2.6 Fixed-bed adsorption . . . . .	7
2.7 Sequential P extraction . . . . .	8
<b>3 Results</b>	<b>9</b>
3.1 Size distribution, LOD, & LOI . . . . .	9
3.2 Aqua regia extraction & X-ray diffraction . . . . .	10
3.3 Shaking test . . . . .	11
3.4 Adsorption kinetics . . . . .	11
3.5 Adsorption isotherms . . . . .	13
3.6 Fixed-bed adsorption . . . . .	14
3.7 Sequential P extraction . . . . .	15
<b>4 Discussion</b>	<b>15</b>
4.1 Physical characteristics & chemical nature . . . . .	16
4.2 Adsorptive behaviour . . . . .	16
4.3 Environmental impact . . . . .	19
4.4 Fit for purpose? . . . . .	19
<b>5 Conclusions &amp; Outlook</b>	<b>20</b>
<b>Declaration of competing interest</b>	<b>20</b>
<b>Acknowledgements</b>	<b>20</b>
<b>References</b>	<b>21</b>
<b>Appendix A Supplementary protocols</b>	<b>24</b>
A.1 Product interference with the SFA . . . . .	24
A.2 Sequential P-extraction; in-house protocol . . . . .	25
A.3 Estimation of flow velocity in shaking test . . . . .	26
<b>Appendix B Supplementary results and measurements</b>	<b>27</b>
<b>Appendix C Personal Communications and Declarations</b>	<b>34</b>
C.1 Summary of the meeting on June 10, 2023 . . . . .	34
C.2 Declaration on the use of generative AI . . . . .	34



# 1 Introduction

## 1.1 Eutrophication

Freshwater biodiversity has been on the decline in the last decades due to chemical pollution, habitat destruction, resource extraction, climate change, and disturbed nutrient cycles [1–3]. These threats to freshwater ecosystems are not isolated, but interact with one another [1].

Harmful algal blooms (HAB) are one symptom of how the disturbances of biosphere integrity and biogeochemical cycles meet. With high light availability, higher temperatures, and high nutrient concentrations in the water column, algae and cyanobacteria can outgrow predatory pressures and proliferate very quickly, thus causing HABs. Cyanobacteria are especially infamous, because various species can produce toxins or cause unpleasant smells [4]. HABs thereby negatively impact ecosystem services like drinking water production, tourism, and aquaculture [5]. HABs have occurred more frequently in the past decades [6] and this trend is likely to continue [4].

Anthropogenic eutrophication is generally considered the main culprit of HABs. It is the artificial enrichment of aquatic ecosystems with nutrients, the macronutrients phosphorus (P) and nitrogen (N) in particular, and the excessive production of organic material that follows [7, 8]. It can cause aquatic ecosystems to transition from a clear to a turbid, algae-dominated state [9]. Algae then dominate the competition for light in the water column and can cause anoxic conditions due to respiration and their quick decomposition [10].

Sources of excessive nutrients into lakes can be external or internal. Among external sources, point and diffuse sources can be differentiated. Point sources include urban centres and wastewater treatment outlets [11]. Diffuse sources are spread out over watersheds, entering surface waters via runoff or atmospheric deposition. Agricultural activities are often the largest contributor to diffuse emissions, via e.g. fertilisation [11–13]. Nutrients applied in excess, especially P, can accumulate in soils, forming a ‘legacy’ nutrient pool. This can then form a source of increased diffuse emissions over several decades, even after drastic changes in agricultural practice reduced nutrient excesses [12, 14, 15]. Nutrients can also enter the water column from within the water body itself. Sediments release P and N into the water column from degrading organic matter as a part of the natural nutrient cycles [16, 17]. This internal loading can be enhanced by anthropogenic inputs, via the accumulation of inputs in the sediment [18, 19], with systems with longer residence times being more susceptible [20–22]. Enhanced internal loads only tend to occur for P, and not N, because the former is

readily taken up by organisms and cannot be lost to the atmosphere via processes analogous to denitrification [17, 18].

## 1.2 Mitigation, prevention, & restoration

There are various measures to mitigate or prevent eutrophication and restore lake ecosystems. These can be categorised as follows: 1) hydrological manipulations, 2) biomanipulation or direct alterations of the ecosystem, 3) external nutrient load reduction, and 4) internal nutrient load reduction [23]. When choosing between measures, it is necessary to map all nutrient fluxes and pools so that the main causes of eutrophication and its symptoms may be addressed [24].

### Hydrological and biological manipulation

Hydrological manipulations are measures that aim to change lake in- and outflows in order to bring about a change in the ecological state of the system. Examples include hypolimnetic withdrawal [25, 26] and high-nutrient source dilution or diversion [27]. Biomanipulation, on the other hand, involves directly altering the ecosystem structure to achieve the same goals. Typical examples include removing benthivorous fish, introducing filter-feeding species, introducing piscivorous fish, reintroducing macrophytes, and harvesting nutrient-rich macrophytes [28–30].

### External nutrient load reduction

Reducing nutrient sources external to lakes is, in principle, the most sustainable of all measures. One could change land management and agricultural practices such that nutrient excesses are prevented, as well as improve wastewater treatment [23, 31]. There also exist so-called ‘P removal structures’, which use filter media to remove phosphorus from flowing surface waters and urban stormwater. [32–34].

The whole landscape may be engineered with the same aims, in particular over the longer term [35, 36]. The (re)construction of buffer zones, sedimentation ponds, and wetlands are typical examples at various spatial scales [35, 36], as well as the alteration of constructed wetland soils or tiledrains with nutrient adsorbent materials [37–39].

### Internal nutrient load reduction

When it comes to reducing internal loads in lakes, three main strategies are typically used. 1) In small, shallow lakes, surficial sediment may be removed wholesale by dredging [23, 26]. 2) A lakebed may also be capped by an inert material, preventing nutrients from entering the

water column [23]. 3) Finally, materials and substances may be added to flocculate particulate nutrient-rich matter out of the water column, adsorb nutrients, or both [23, 24, 40]. Furthermore, some adsorbents may also act as a sediment-capping material [40, 41] or flocculant ballast [42].

Nutrient adsorbents typically primarily target P, rather than N [24, 40]. P is the main limiting nutrient in most lakes; co-limitation with N is also common, but lakes are only infrequently limited by N [43]. P reduction, though not universally effective [22], has had success in mitigating the symptoms of eutrophication [24]. As a result, chemical inactivation or sequestration of P is still considered an effective method for combating HABs and improving water quality.

In a comprehensive summary of adsorbent materials, Douglas *et al.* [40] distinguished 4 broad categories of nutrient sorbents, united by being enriched with carbonates, Fe, Al, rare earth metals like La, or some mixture. Typically, they have maximum adsorption capacities (MAC) between around 1 to 100 mg P g<sup>-1</sup>, though most have capacities below 20 mg P g<sup>-1</sup> [24]. Depending on the environmental conditions in any given lake, adsorbents can be more or less appropriate for use [24, 40]. Environmental conditions such as redox status, pH, or salinity can affect the solubility of an adsorbent. Nowadays, Al salts, Al-(oxyhydr)oxides, or La-modified materials are most often used, due to their relative insensitivity to these conditions [23].

### 1.3 In-stream phosphorus adsorption

From the above discussion, we can identify a gap in the available strategies. Once nutrients end up in the surface waters, they are largely lost until they find their way into lakes, where they cause eutrophication. The majority of measures that act between the source and the endpoint tend to involve larger-scale alterations in the landscape such as the (re)construction of streams or wetlands [36], or management structures such as the P-removal structures [32, 33]. Wetland reconstruction also provides other benefits, but they require a lot of space and are typically costly [23]. P-removal structures are much smaller and cheaper, but still more expensive than in-lake P-removal with adsorbents [34, 44]. Edge-of-field filter structures in agricultural catchments with various filter materials have also been studied, though again, these structures are often built into the landscape [39]. As such, there is a need for more flexible strategies that specifically target the nutrients in-stream, without requiring the substantial monetary and spatial costs. One can expect that such a strategy can speed up the recovery of aquatic ecosystems, even with ongoing legacy diffuse emissions. Furthermore, it would reduce the long-term

need for more invasive repeated in-lake measures, which are arguably a necessity in areas with large intensive agricultural industries, like the Netherlands [41].

In the last few years, two companies have brought products on the market that claim to do just what is outlined above. Water Warriors Inc. and SePRO Corporation have put out Phosflow™ and EutroSORB® F respectively [45, 46].

Phosflow™ is a medium made of solid, near-spherical pellets, as shown in Figure 1 a), meant to adsorb P from running waters up to an MAC of 26.4 mg P g<sup>-1</sup> [45]. According to Water Warriors Inc, it 'can be implemented as a filter media to remove phosphate from a variety of environmental matrices such as lakes, streams, drains and channels.' One available safety data sheet lists MgCO<sub>3</sub> and Al<sub>2</sub>O<sub>3</sub> as the main constituents [47].

EutroSORB® F, shown in Figure 1 b), is a filter material made with the same aim as Phosflow™ [46]. Beyond a claimed P-binding MAC of approximately 10 mg P g<sup>-1</sup>, not much is publicly available about this product. However, a potentially related patent application put out by the SePRO Corporation in the United States of America claims a composite material consisting of a 'nutrient-binding ingredient' and a 'biogenic additive', which should together lead to synergistic P adsorption [48]. Various combinations of ingredients are claimed in the patent, some of which are known P-binders, like aluminium minerals. Aluminium-based constituents may be expected (Fuhrmann, personal communication; see Appendix C.1).

If Phosflow™ and EutroSORB® F (from here on collectively referred to as 'the products') function as claimed, they would fit neatly into the strategical gap identified earlier, and they could nicely complement other mitigation strategies, like changing land management practices and in-lake measures [49]. However, it would not be the first time that ineffective lake restoration technologies are commercially available, as illustrated in the Netherlands by Lüring & Mucci [41]. In the case of these two products, there is very little public information available, so it is vital that these technologies are tested independently.

Given all the above, we can say that the performance and properties of two commercially available in-stream nutrient sorbents that could close a vital link in the chain of eutrophication mitigation strategies are largely unknown. From this problem statement, a main research question follows:

*What are the adsorptive characteristics of Phosflow™ and EutroSORB® F and are they fit for purpose?*

In order to answer this question, the following aspects about these products will be studied: 1) their



**Figure 1 – Two in-stream phosphate adsorbents** – The two products side by side. (a) shows Phosflow pellets™ and (b) shows EutroSORB® F. These pictures were taken by the author.

physical characteristics, in particular with regards to their stability in water; 2) their chemical nature in terms elemental and mineral composition; 3) their adsorptive behaviour under static equilibrium and under flowing conditions; 4) the general environmental impact of their use with regard to general water chemistry properties. These may be formulated into more specific sub-research questions.

1. What are the physical characteristics of the products, in particular with regards to their stability in water?
2. What is the chemical nature of the products, in terms of elemental and mineral composition?
3. What is the adsorptive behaviour under static equilibrium and under flowing conditions?
4. What changes in the general water chemistry properties occur as a result of the usage of the products? I.e., what is the further environmental impact of using these products?

Information provided on the websites of the products and the found patent give a basis for setting up some hypotheses. As this information is limited, especially with respect to EutroSORB® F, formulations of most prior hypothesis must be kept vague or unspecified. First, some general hypotheses: both products are stable in water; they can adsorb phosphate, both in static and flowing media; they have a limited expected environmental impact beyond adsorbing phosphate; the formation of phosphate minerals will occur. The specific meaning of words like 'limited' and 'stable' or not too important, but should invoke a sense of what realm of endpoints the research questions will deal with.

Now we come to those hypotheses that can be based on what is known about the materials, as laid

out in earlier sections. Regarding Phosflow™: we may suspect its composition to be dominated by a combination of magnesium carbonates ( $\text{MgCO}_3$ ) and aluminium oxide ( $\text{Al}_2\text{O}_3$ ), with a maximum P adsorption capacity of around  $26.4 \text{ mg P g}^{-1}$ . Regarding EutroSORB® F: we may suspect that they are made of some known phosphate adsorbent mixed with one or more other ingredients, some possibly of biogenic origin or including a substantial amount of Al. It may have a maximum P adsorption capacity of around  $10 \text{ mg P g}^{-1}$ .

## 2 Methods & Materials

In order to determine whether the products EutroSORB® F and Phosflow™ are fit for purpose, several smaller experiment were carried out. Figure 2 gives a general overview of the main methods employed. The main focus was on P adsorption experiments. Furthermore, several other endpoints were investigated to estimate the further environmental impact that the products may have when in use. Generally, these were pH, electrical conductivity (EC), and turbidity or suspended solids. Placing these two main aspects in context requires having an understanding of what the physical properties and chemical make-up of the products are. They should provide ample information to interpret the observed behaviour of the products.

The main chain of different experiments started with the shaking test. Its objective was to provide qualitative information on the resistance of products to mechanical abrasion. Furthermore, it allowed for determining a shaking regime with which the products could be

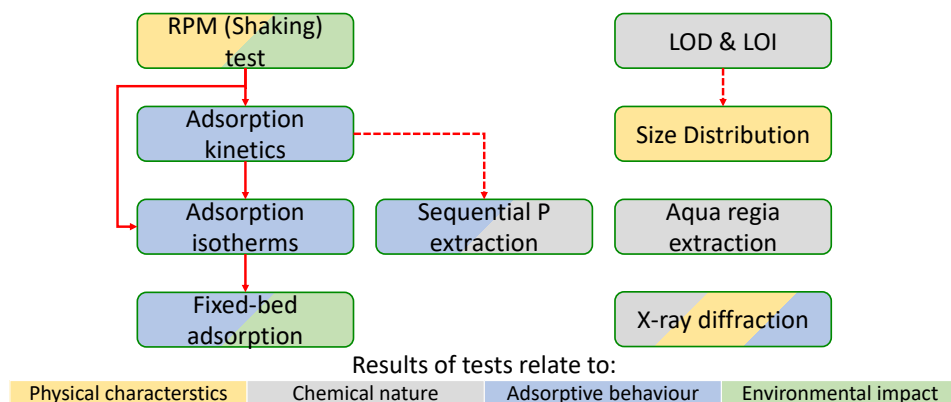


**Figure 2 – Overview of the methods** – An overview of the main methods that were employed here and how they fit together. The arrows indicate that some results are used in the design of another experiment. In the case of the bold arrows, this relates to numerical values or considerations of how to practically carry out the next experiment in the chain. In the case of the broken arrows, some material produced in one experiment is directly used in another. All boxes in the figure are coloured according to the domain of interest the results relate to. Yellow relates to the physical properties of the materials, blue to the adsorptive behaviour of the products, green to further environmental impacts that may be expected when the products are used, and grey to the chemical nature of the products

mixed without destroying the bulk while in suspension. With this information, the room-temperature adsorption kinetics could be determined. The time it takes to reach equilibrium could then, in turn, be used to establish the timeframe needed to perform further batch-adsorption experiments. The main batch-adsorption experiments that followed were done to construct adsorption isotherms, and thereby determine equilibrium adsorption behaviour. With those results in mind, fixed-bed adsorption experiments were done to test the products' capabilities in flowing conditions, thereby determining whether the products are actually fit for their intended purpose. Several of these parts involve model-fitting and parameter estimation. For this, linear least squares procedures implemented in R version 4.2.3 were used [50], unless otherwise described in the methods.

Alongside these experiments, various analyses were performed to characterise the products. Loss on drying (LOD;  $\sim 105^{\circ}\text{C}$ ) and loss on ignition (LOI;  $\sim 550^{\circ}\text{C}$ ) of the products were determined to get a sense of their room-temperature moisture content and whether they contain more volatile constituents. The X-ray diffraction (XRD) spectra of the products were measured to ascertain the minerals present in them. Finally, aqua regia destruction followed by induced-coupled plasma-mass spectrometry (ICP-MS) and ICP optical emission spectrometry (ICP-OES) were performed to determine the elemental composition of the products.

Several endpoints were measured across various different experiments, for which the same instruments were used. To measure pH and EC, a SenTix® 41 pH-electrode (WTW®) and a Tetracon® 325 (WTW®)

were used, combined with various multimeters (pH 3110, pH 320, pH/Cond 340i, pH cond3320; WTW®). For Turbidity, a 2100P turbidimeter (Hach®) was used respectively. Samples were analysed for soluble reactive P (SRP) and total P (TP) using a segmented flow analyser (SFA) (Skalar, SAN+ System), following NEN-EN-ISO 15681-2:2005 [51].

For SRP analysis, samples were filtered. All samples and filtrates for TP and SRP analysis were stored at  $-20^{\circ}\text{C}$  until analysis, unless indicated otherwise. At the start of the project,  $0.45\ \mu\text{m}$  syringe filters (cellulose acetate; Whatmann™, 10462600) were used, while later experiments used  $0.2\ \mu\text{m}$  membrane filters (cellulose nitrate; Whatmann™, 10401314) mounted in a vacuum pump (Shanghai Eyela Co., Ltd, Aspirator A-1000S). This was done to pre-emptively reduce interference from the products after filtration (see subsection A.1 for more details). Extensive use was made of 50-mL centrifuge tubes (VWR®, 525-1113) and 15-mL centrifuge tubes (VWR®, 525-0605). For dry weight analysis, aluminium dishes (VWR®, 611-1371) were generally used, unless indicated otherwise. All liquid samples were stored in 50-mL polyethylene (PE-LD) bottles (Kautex™, 2000770528). Other materials that were used are indicated under the subsection where their use is described. This concerns materials that were only used for one experiment.

For all adsorption experiments,  $\text{K}_2\text{HPO}_4$  (Merck KGaA; 1.05104.1000) was used. When constructing the adsorption isotherms, KCl (Merck KGaA, 1.04936.0500) was also used. The following chemicals were used for the sequential P extraction: a BD-reagent (containing  $0.11\ \text{M}\ \text{Na}_2\text{S}_2\text{O}_4$  (Merck KGaA, 1.06507.0500) and  $0.11$

M NaHCO<sub>3</sub>(Merck KGaA, 1.06329.1000)); 0.1 M NaOH (Merck KGaA, 1.06498.1000); 0.5 M HCl, diluted from stock (Merck KGaA, 1.00317.100); 2M H<sub>2</sub>SO<sub>4</sub>, diluted from stock (Merck KGaA 1.00731.1011)

Data analysis was done using Rstudio version 4.2.3 with its native packages [50], and figures were created using the 'ggplot2', 'ggpubr', 'patchwork', and 'ggpattern' packages [52–55]. Data analysis was further facilitated by the 'tidyverse', 'rstatix', and 'hydroGOF' packages [56–58].

## 2.1 Size distributions, LOD, & LOI

Given EutroSORB® F's heterogeneous nature, understanding the size-distribution of the products would be helpful in further investigations. Thus, known amounts of product were deposited into a sieving tower, containing six sieves with different pore sizes. These are, in decreasing order: 4.8, 2.8, 2.0, 1.0, 0.5, and 0.180 mm. After sieving, the material left on each sieve was collected and weighed. The fraction of material smaller than 0.180 mm were inferred by closing the mass balance, though potential accidental losses were also confounded into this size fraction, thereby forming an 'Error/Rest'-fraction. Sieving was done five-fold for both products.

The large EutroSORB® F 'mode' was also separated by hand and the fraction of the total determined, with six replicates. Such separation was done in further characterisation as well, so this simple check can be compared to the more general size-distribution.

The presence of moisture and/or hydrous minerals at room temperature conditions may be inferred from the loss on drying (LOD). Similarly, substantial loss on ignition (LOI) indicates the presence of organic matter such as cellulose or, to a lesser degree, minerals that can degas at higher temperatures.

Thus, known amounts of both product were dried at 105 °C for 64 h and subsequent percentual mass losses calculated as in Equation 1. Here,  $M_0$  (g) is the initial mass and  $M_{dry}$  (g) is the mass after drying. After, the dried products were ignited at 550 °C for 3 h, and then mass losses were calculated as in Equation 2. There,  $M_{ash}$  (g) is the mass after ashing. LOD- and LOI-analysis was done with 5 replicates. After ashing and weighing, the samples were stored at room temperature in a desiccator for around a week.

$$LOD = \frac{M_0 - M_{dry}}{M_0} \cdot 100\% \quad (1)$$

$$LOI = \frac{M_{dry} - M_{ash}}{M_{dry}} \cdot 100\% \quad (2)$$

Finally, after the storage period, the samples were weighed once more, aggregated, and sieved just like the

non-dried samples. The mass fractions of the total input for each size fraction were compared with the mean non-dried fractions.

## 2.2 Aqua regia extraction & X-ray diffraction

In order to determine the elemental composition of the products, the products were chemically destroyed, and the resultant solution analysed. EutroSORB® F was separated by hand, and the two fractions were analysed separately. Thus, 3 samples for analysis arose: the large EutroSORB® F mode, the small EutroSORB® F mode, and Phosflow™.

0.5 g of the samples was ground and suspended in aqua regia (HNO<sub>3</sub>/HCl, 1:3 molar ratio), which was then heated overnight at boiling point (~108°C). The cooled resultant solutions were filtered. One part was analysed using induced-couple plasma mass spectrometry (ICP-MS) (Thermo Element 2, Thermo Fisher Scientific) for As, Cd, Cr, Cu, La, Ni, and Zn. Another part of the solutions was analysed using ICP-optical emission spectrometry (ICP-OES) (Thermo iCAP 6500 DV, Thermo Fisher Scientific) for Al, Ca, Fe, K, Mg, Mn, Na, P, Pb, S, and Si. Destruction and analysis were carried out by the Wageningen University & Research Soil Chemistry Laboratory (CBLB) [59]. Based on the findings of XRD-analysis, maximum mass fraction of dominant minerals could be inferred.

To determine the mineral structure of the products before and after use, X-ray diffraction (XRD) was used. This was done with 3 samples from each product, with the two modes of EutroSORB® F being separated before analysis: untreated, dried at 80 °C for 2 days, incubated in 2 L of solution with 100 mg P L<sup>-1</sup> for two weeks and then dried at 80 °C for 2 days. The mixtures in which the products were incubated were analysed for SRP and TP before and after incubation. For SRP analysis, solution was filtered through a 0.2 µm membrane filter. Thus, the P adsorbed per unit dried weight was calculated.

XRD analysis was then performed on the thus acquired samples using a Bruker D8 Advance diffractometer (Bruker AXS), with Cu-Kα radiation generated at 40 kV - 40 mA (wavelength of 0.154 nm). The angular range used was 10 to 90° (2θ) with a step size of around 0.02° at 0.1 s per step and with a variable slit opening (Fixed Sample Illumination 10 mm).

The found diffractogrammes were then identified by comparing the found patterns with the crystallographic open database(COD) [60]. Analysis was carried out by the WUR Environmental Technology group.

### 2.3 Shaking test

To gather a sense of the physical stability of EuroSORB® F and Phosflow™, they were shaken over 7 days using different shaking regimes. After this, mass losses, EC and pH were determined. The results from this test aided in determining the shaking regime used in further tests.

Around 2 g of product was applied to 40 mL of deionised water (DIW), in triplicate, which was shaken according to one of 9 regimes. These are a combination of three different shaking times and strengths. Shaking durations of 1, 3, and 7 days were chosen. The three different shaking regimes were: leaving the mixture still ('Still'), putting it on a stirring table at 100 rounds per minute (RPM) ('Weak'), or putting it on a shaker table at 140 RPM ('Strong').

While the samples were shaking, aluminium floats and 0.8 µm fine-grained glass-fibre (GF/C) filters were prepared. The latter were washed using DIW, and both were pre-dried at around 110 °C for at least 2 hours.

Once a treatment had finished, pH (-) and EC (µS cm<sup>-1</sup>) in the mixtures were recorded. These mixtures were then sieved through a 0.180 mm sieve and the effluent was collected. The bulk of the material left in the sieve was deposited in aluminium floats. Between samples, the sieve and funnel were washed with DIW. All of the effluent was filtered using a vacuum pump and a GF/C filter. Finally, the captured bulk material and filters were dried at around 110 °C for at least 16 hours.

The total mass loss was determined from the difference between the dried bulk mass and the bulk mass put into the mixtures. This number was corrected for the LOD by subtracting the latter from the total mass loss: a representation of the total mass percentage lost due to shaking the mixtures  $\Delta M_{shake}$  (%). The calculation was done as in Equation 3:  $M_i$  (g) is the product mass initially put into a mixture,  $M_{dried}$  (g) is the dried bulk mass. LOD is given in Equation 1.

$$\Delta M_{shake} = \frac{M_i - M_{dried}}{M_i} \cdot 100\% - \text{LOD}\% \quad (3)$$

Dry suspended solids gathered on the filter after shaking were determined from the mass differences between the mass of an empty filter ( $M_{i,filter}$  (g)) and the same used filter ( $M_{dried,filter}$  (g)), as in Equation 4. There,  $\Delta M_{SS}$  (%) is the mass loss percentage as the suspended solids fraction. These were not corrected for LOD. With all samples gathered and pre-analysis done, then, means and 95% confidence intervals for every treatment across the two products were estimated.

$$\Delta M_{SS} = \frac{M_{dried,filter} - M_{i,filter}}{M_{i,filter}} \cdot 100\% \quad (4)$$

To finish the analysis and determine the significance of either time spent being shaken  $t_{shake}$  (d) and at what RPM (-) on all endpoints, multi-linear regression was done. Such a model is shown in Equation 5. There,  $Y$  is a representative of some endpoint, being  $\Delta M_{shake}$  (%),  $\Delta M_{SS}$  (%), pH (-), or EC (µS cm<sup>-1</sup>).  $A$ ,  $\vec{B}$ , and  $\vec{C}$  are coefficients, the last two being vectors. This is because the shaking regime must be introduced as a 3-element vector  $\vec{RPM}$  due to it being a qualitative factor. All possible models are made, so every combination of terms given in Equation 5, and compared with one another using ANOVA. The least complex model with the lowest adjusted  $R^2$  is reported. If there were two or more models that are statistically equivalent, the simplest model was chosen.

$$Y = At_{shake} + \vec{B} \cdot \vec{RPM} + t_{shake} \vec{RPM} \cdot \vec{C} \quad (5)$$

### 2.4 Adsorption kinetics

In order to determine the room-temperature adsorption kinetics of EuroSORB® F and Phosflow™, an adsorption-kinetics experiment was conducted over the course of 3 weeks. 2 triplicates of DIW-based K<sub>2</sub>HPO<sub>4</sub> solutions were made, containing 0.513 L with 50.7 mg P L<sup>-1</sup> and 1 g EuroSORB® F, the other containing 0.533 L DIW with 130.8 mg P<sup>-1</sup> and 1 g Phosflow™. If the hypothetical MACs of around 10 and 26.4 mg P g<sup>-1</sup> hold, around 20% of the P in solution should be removed.

2 positive controls were prepared containing the same P concentration as either product-solution mixture, but without product. Finally, two blank mixtures, with neither P nor product, were prepared. All mixtures were made in 0.5 L flasks and shaken in upright position at 100 RPM on a shaker table.

At the end of every incubation interval, the content of each bottle was sampled. 90 µL were taken from the EuroSORB® F mixtures, and 35 µL were taken from the Phosflow™ mixtures and mixed with 50 mL DIW. These dilutions were filtered using 0.45 µm syringe filters, and analysed for SRP. The positive controls were treated as their analogous mixtures, and the blanks were treated as the EuroSORB® F mixtures. With sampling complete, pH and temperature (°C) were measured in every mixture.

The initial experiment ran for 8 days, after which the bottles were no longer shaken. However, the sampling period was extended for 1.5 more weeks. At the end of this second period, dry weight analysis was performed on the bulk material. The same methods were used here as described for the shaking test. The remaining dry bulk material was then used for sequential P extraction, as described in subsection 2.7.

Adsorption  $Q$  ( $\text{mg P g}^{-1}$ ) onto the products was calculated according to Equation 6. Here,  $C_0$  ( $\text{mg P L}^{-1}$ ) is the SRP measured in a bottle at time  $t = 0$  d,  $C_t$  ( $\text{mg P L}^{-1}$ ) is the SRP measured in a bottle at a later time  $t$ ,  $V$  (L) is the volume present in the bottle at time  $t$  (d), and  $M$  (g) is the amount of product put into a bottle. Potential mass losses of the products in the mixtures are neglected for the sake of simplicity, since Figure 6 shows low mass losses for similar a shaking regime ( $\leq 2.5\%$  for EuroSORB®F and  $< 1\%$  for Phosflow™).

$$Q_t = (C_0 - C_t) \frac{V}{M} \quad (6)$$

Then, a pseudo first-order model was fitted to the data of each bottle, as in Equation 7. Though only an empirical model, the parameters have a straightforward physical interpretation.  $Q_{\max}$  ( $\text{mg P g}^{-1}$ ) is the MAC given the experimental conditions, and  $k$  ( $\text{d}^{-1}$ ) may be interpreted as an adsorption rate. The mean of the model parameters gained by fitting Equation 7 to each bottle was calculated for each mixture type. The data from the extended measurement period was used, given that pH measurements indicated that chemical conditions in the bottles were stable after the initial experiment (see Figure B.2 b)).

$$Q_t = Q_{\max}(1 - \exp(-kt)) \quad (7)$$

## 2.5 Adsorption isotherms

Further batch adsorption experiments were carried out with the objective of constructing adsorption isotherms. Thus, the products EuroSORB® F and Phosflow™ were suspended into 7 solutions with different concentrations of  $\text{P-PO}_4$ : 0, 1, 10, 25, 65, and 100  $\text{mg P L}^{-1}$ . To homogenise the  $\text{K}^+$  concentrations in all solutions, KCl was added to increase the concentration of  $\text{K}^+$  to that in the solution with the highest  $\text{P-PO}_4$  concentration. The pH in the solutions was altered to be around 7 ( $\pm 0.5$ ) using 0.1 M HCl, 1 M NaOH, and 6 M HCl solutions. Samples were isolated from the main stock solutions for TP and SRP analysis. For SRP analysis, samples from the solutions were filtered using 0.2  $\mu\text{m}$  membrane filters.

The batches consisted of 0.5 g EuroSORB® F suspended in 200 mL solution and 0.1 g Phosflow™ suspended in 100 mL solution, all prepared in triplicate. EuroSORB® F was more challenging to sample consistently, compared with Phosflow™, so more material was used to prevent inconsistent batches. If hypothetical MACs hold, reduction in the total available P in the batches should be similar, hence the different product-solution ratios. Treatments with 0  $\text{mg P L}^{-1}$  and no product, as well as pure distilled water were included

in triplicate as control groups. The mixtures with EuroSORB® F and Phosflow™ were shaken at 100 RPM on a stirring table for 6 and 13 days respectively, being informed by the timescales shown in Figure 7. After the shaking period, pH, EC, and turbidity (NTU) of the mixtures were measured. Then, samples were taken and half was filtered with 0.2  $\mu\text{m}$  membrane filters for SRP analysis, and the rest was kept for TP analysis.

The SRP and TP concentrations were corrected for the average of the measured values in batches without P and product, and adsorption isotherms were fitted using non-linear regression. Here, the Langmuir model was used, as shown in Equation 8. There,  $C$  ( $\text{mg P L}^{-1}$ ) is the equilibrium ortho-phosphate concentration and  $K$  ( $\text{L mg}^{-1} \text{P}$ ) is the Langmuir coefficient. The adsorption was calculated as in Equation 6, for both the results from the TP and SRP analyses.

$$Q = Q_{\max} \frac{KC}{1 + KC} \quad (8)$$

## 2.6 Fixed-bed adsorption

A fixed-bed adsorption experiment was carried out to test the performance of the products under flowing conditions. A schematic of the fixed-bed setup is shown in Figure 3.

The beds were 1.2-cm diameter plastic tubes with flexible plastic mesh (supplied by SePRO Co.; pore size  $\sim 0.4$  mm, B.C. Fuhrmann, personal communication) fastened to the bottom. No information was available on the average or normative pore size of the mesh. There were 6 beds: 2 with 0.5 g Phosflow™, 2 with 0.75 g EuroSORB® F, and two were left empty. Bed thicknesses were around  $9 \pm 1$  mm, i.e., although the amounts of material were different, bed thicknesses were similar (within  $\sim 10\%$ ).

Two different solutions were pumped through a set of three beds each, using a multichannel peristaltic pump (Watson-Marlow type 202) at a mean flow rate  $\bar{q}$  of  $2.16 \text{ mL min}^{-1}$  (ranging from  $1.05$  to  $2.93 \text{ L min}^{-1}$ , see also Figure B.1). The first was distilled water with  $1 \text{ mg P L}^{-1}$ , and the second was water from a local

**Table 1 – Fixed-bed adsorption intervals** – An overview of the timestep intervals in the fixed-bed adsorption experiment, with indicative values of the flow-time, and mean flow rate.

Interval	$t_{\text{flow}}$ (h)	$\bar{q}$ ( $\text{mL min}^{-1}$ )
1-7	0.75	2.09
8-9	2.9	2.37
10	6.5	2.30
11-12	14.75	2.34
13-14	21.2	1.91
15	15.5	2.52

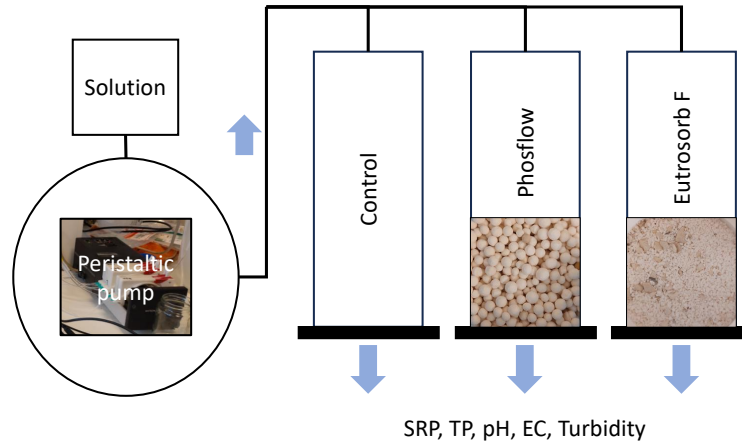


**Figure 3 – Fixed-bed setup** – Schematic of the fixed-bed setup for one solution. The solution is pumped using a multichannel peristaltic pump into three separate beds, one control without product, one with 0.5 g Phosflow™, and one with 0.75 g EutroSORB® F. The effluents are all analysed for SRP, TP, pH, EC, and turbidity.

pond spiked with around  $1 \text{ mg P L}^{-1}$ . This water was gathered between October 27 and December 4, 2023, on Wageningen University & Research grounds at (Lat.: 51.988164, Long.: 5.666855).

Every sampling interval involved passing the solutions through the beds, capturing the effluent, and measuring a collection of endpoints. Interval numbers, indicative values for flow time for each interval, and mean flow rate among all outlets within those intervals are given in Table 1. At the start of every interval set, pH, EC, dissolved oxygen ( $\text{mg O}_2 \text{ L}^{-1}$ ) (CellOx 325 probe; WTW®), and turbidity were measured in the influent. At the end of every interval, pH, EC, turbidity, flow time  $t_{\text{flow}}$  (min), and effluent volume (L) were measured. Based on these last two, interval-mean flow rates for every outlet were estimated; these are shown in Figure B.1. Finally, approximately 50 mL effluent was collected, half of which was filtered using a  $0.2 \mu\text{m}$  membrane filter, for SRP and TP analysis. The spiked pond-water effluents were also analysed for total nitrogen (TN).

The TP and SRP time series were used to fit a model of the form of Equation 9, with mean influent P concentration  $C_0$  ( $\text{mg P L}^{-1}$ ) and effluent P concentration  $C$  ( $\text{mg P L}^{-1}$ ) and time  $t$  (min).  $b$  (-) and  $m$  ( $\text{h}^{-1}$ ) are model parameters. Equation 9 is the form that various fixed-bed adsorption models take when linearised [61, 62]. Here, the Bohart-Adams model with accompanying parameters was used, as in Equation 10 and Equation 11. There,  $k_B$  ( $\text{mg P L}^{-1} \text{ h}^{-1}$ ) is a rate constant, and  $M$  (g) is the amount of product in the bed. Equation 11 can directly be used as an estimate of the fixed-bed MAC. The error on this figure can then be estimated via linear error propagation. For this, the following errors were assumed  $\sigma_M = 0.001 \text{ g}$ ,  $\sigma_{C_F} = 0.02 \text{ mg P L}^{-1}$ , and  $\sigma_q = 0.145 \text{ mL min}^{-1}$ .  $\sigma_M$  and  $\sigma_{C_F}$  are based on the

detection limits of the analytical balance and P-analysis respectively.  $\sigma_q$  is based on the accuracy of a regular ruler to measure the effluent volume in a rectangular box (0.5 mm).

$$\ln \left[ \frac{C_0}{C} - 1 \right] = b - mt \quad (9)$$

$$k_B = \frac{m}{C_0} \quad (10)$$

$$Q_{\text{max}} = \frac{C_0 \bar{q}}{mM} \ln [e^b + 1] \quad (11)$$

Cumulative adsorbed P  $Q_{\text{cum},t}$  was calculated after every time step using Equation 12 [63]. The sum runs from time step  $i$  up to time step  $N_t$ . Here,  $\Delta t_i$  (min) is the flow time for time step  $i$ . All other symbols are the same as before, but at a discrete time step  $i$ . This calculation was done using both experimental results and model predictions based on Equation 9. When calculating  $Q_{\text{cum},t}$  from model predictions, series mean  $q$  and  $C_0$  were used.

$$Q_{\text{cum},t} = \frac{1}{M} \sum_{i=1}^{N_t} (C_{0,i} - C_i) q_i \Delta t_i \quad (12)$$

## 2.7 Sequential P extraction

Sequential P extraction on the solid products provides information about the different P-pools in a sample. Consequently, the processes and substances controlling adsorption and precipitation can be disentangled to some degree. Here, dried bulk material from the kinetics experiment were used. Given the large P concentrations that these materials were exposed to, and equilibrium was reached, one may expect that the products produced

**Table 2 – P-fractions in sequential extraction** – Overview of the different extractions employed in the sequential P-extraction and their rough correspondence to different pools of P in the material.

Phase	Solution	P-analysis	Corresponding sorbent substrate
1	O <sub>2</sub> -free distilled water	SRP	Fe & CaCO <sub>3</sub> surfaces; loose
2	O <sub>2</sub> -free 0.11 M Na <sub>2</sub> S <sub>2</sub> O <sub>4</sub> /NaHCO <sub>3</sub> (BD)	SRP & TP	Fe-hydroxides & Mn-compounds
3	0.1 M NaOH	SRP & TP	Clay-minerals & metal(Al)-oxides
4	0.5 M HCl	SRP & TP	Carbonates & P-containing minerals
5	2 M H <sub>2</sub> SO <sub>4</sub>	SRP	Refractory P

were essentially saturated with P. Alongside the saturated products, in triplicate, the sequential extraction was also performed on samples of unused product and blanks without product, also in triplicate.

The whole procedure follows a protocol based on the work described in Paludan & Jensen [64]. The modified protocol, along with extra relevant alterations, can be found in Appendix A.2. All extractions except the last one were carried out at 19 °C, while continuously shaking at 140 RPM, laid horizontally on the shaker table. Every such extraction was followed by centrifugation at 2800 RPM for 10 minutes, after which the supernatant was decanted. Any filtering mentioned was done using 1.2- $\mu$ m glassfiber filters (GF/C). Table 2 gives an overview of the whole extraction procedure: the phase number, what extraction reagent was used, the P-analysis done with the final solutions, and some indicative correspondences to P-pools in the materials.

Measured P concentrations were corrected for dilution factor, then blanks. From the differences between TP and SRP measurements, soluble non-reactive phosphorus (SNRP) could be calculated. This yields a total of 7 unique P-concentrations from associated P-pools. Then  $Q$  was calculated for all 7 according to the protocol in Appendix A.2.

Furthermore, for every solution-analysis pair indicated in Table 2, pairwise comparison of means was done for adsorbed P between the materials: untreated products, and treated products. Thus, for every pool, untreated products, and treated products were compared. The same was done for the measured concentrations, for which the blanks were also included. Given the low sample size per group ( $N = 3$ ), non-normality was assumed and non-parametric test were used. The comparisons were done using Kruskal-Wallis tests followed by Dunn's tests with uncorrected  $p$ -values.

## 3 Results

### 3.1 Size distribution, LOD, & LOI

The upper panel in Figure 4 shows the size distribution of the unused, untreated products. Phosflow™ is relatively

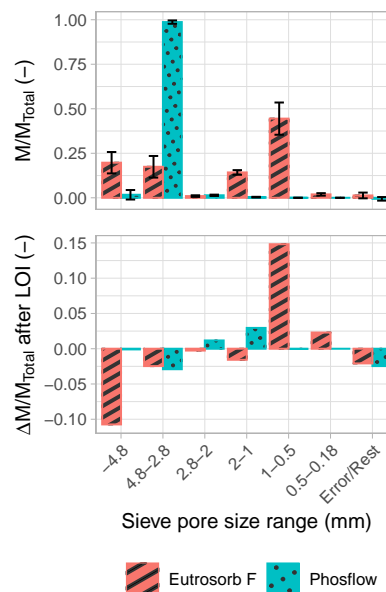


**Figure 4 – Size distributions & changes after LOI** – The upper panel shows size distributions of EutrosORB® F and Phosflow™ with standard deviations ( $N = 5$ ). The lower panel shows the changes in the mass fraction after LOI with respect to the means of the untreated distribution.

uniform, with more than 95% being between 2.8 and 4.8 mm in diameter. EutrosORB® F shows a clear bimodal separation, with around 38% being larger than 2 mm, and the rest smaller than 2 mm. Visually, the former corresponds to the larger irregular material in the product, while the latter corresponds to the visually uniform white material. In the size fraction running from 2 to 1 mm, there is a mix of the two visual fractions.

**Table 3 – LOD & LOI** – Loss on drying (LOD) and loss on ignition (LOI) of both EutrosORB® F and Phosflow™ with standard deviations ( $N = 5$ ).

Product	LOD (%)	LOI (%)
Phosflow	$2.4 \pm 0.8$	$9.5 \pm 0.4$
EutrosORB F	$6.7 \pm 0.4$	$6.1 \pm 0.4$

**Table 4 – Aqua regia destruction results** – Results of the aqua regia destruction and analysis, split according to major and trace elements. Inferred mineral fractions based on the total found major elements and the results of subsection 3.2 are also indicated. Some elements were measured below the limit of detection in all samples (As, LOD:  $0.1 \mu\text{g g}^{-1}$ ; K, LOD:  $70 \mu\text{g g}^{-1}$ ; Pb, LOD:  $3 \mu\text{g g}^{-1}$ ), denoted as ND.

Element	Major elements ( $\text{mg g}^{-1}$ )				Inferred minerals ( $\text{mg g}^{-1}$ )						
	Al	Ca	Mg	Na	AlOOH	CaCO <sub>3</sub>	MgCO <sub>3</sub>	MgO			
Limit of detection	0.04	0.04	0.01	0.1							
Phosflow™	320	0.381	4.28	2.94	711	0.951	14.8	7.09			
Small EutroSORB® F	302	16.1	0.091	1.92	671	40.2	0.316	0.151			
Large EutroSORB® F	0.631	390	1.73	0.393	1.40	973	6.01	2.87			
Element	Trace elements ( $\mu\text{g g}^{-1}$ )										
	Cd	Cr	Cu	Fe	La	Mn	Ni	P	S	Si	Zn
Limit of detection	0.05	0.8	0.6	30	-	1	1.6	3	30	-	18
Phosflow™	0.06	1.4	1.4	110	0.51	14.3	2.0	-	-	75.3	71
Small EutroSORB® F	ND	ND	0.6	89	6.32	ND	ND	-	-	66.7	22
Large EutroSORB® F	ND	3.4	ND	145	0.91	7.7	ND	65	159	232	ND

When sorting EutroSORB® F by hand, the split between large and small modes lies around the same value reported above. The first, second, and third quartiles of the large fraction in EutroSORB® F are 26.5, 41.9, and 44.1% ( $N = 6$ ). The median roughly corresponds to larger fractions in the upper panel of Figure 4, potentially including similar material that may be included in the 2-1 mm pore size range. For the aqua regia extraction and XRD analysis such by-hand separation occurred, so there around 41% was taken from the bulk as 'large' EutroSORB® F.

Table 3 shows the LOD and LOI of the two products. For EutroSORB® F, the two take on around 6.7% and 6.1%, while for Phosflow™, they are around 2.4% and 9.5%. As such, room-temperature EutroSORB® F contains more water, but Phosflow™ more material that can release volatiles at 550°C.

The lower panel in Figure 4 shows the changes in the mass fraction in each size category after LOI with respect to the averages in the untreated distribution, so the distribution seen in the upper panel. Differences in Phosflow™'s distribution are small ( $<0.03$ ). Changes in EutroSORB® F's distribution suggest an increase in the relative importance of the smaller fractions compared to the larger fractions. Given that mass is lost, it may be assumed that the larger size fractions lost most mass and that losses in the fractions 1-0.5 and 0.5-0.18 mm is much smaller. However, note that changes after LOI are similar to the error interval of the fractions of the undried product.

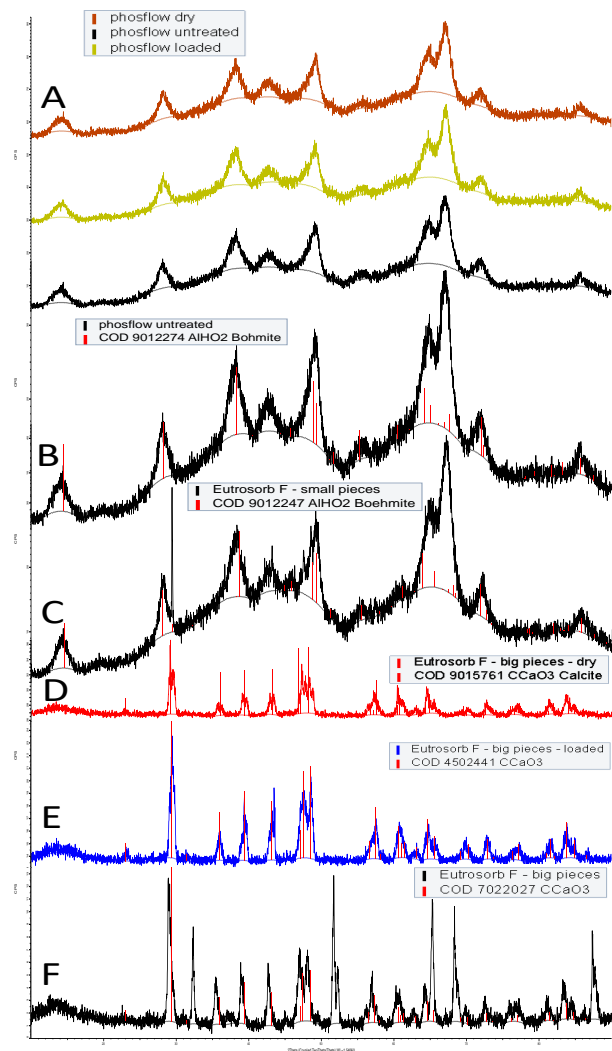
### 3.2 Aqua regia extraction & X-ray diffraction

Table 4 shows the results of the aqua regia destruction and analysis. As noted before, EutroSORB® F was separated by eye, the large mode being about 42% of the total product by mass (see subsection 3.1). Phosflow™ and the small EutroSORB® F mode are dominated by Al and contain appreciable amounts of Mg and Ca respectively. Based on mineral inference (see Figure 5), they contain around 71 and 67% böhmite ( $\gamma\text{-AlOOH}$ ). The large EutroSORB® F mode is dominated by Ca, being almost exclusively calcite ( $\text{CaCO}_3$ ) (97%). Furthermore, Na forms a noticeable fraction of Phosflow™ (0.29%) and small EutroSORB® F (0.19%).

All three materials contain trace amounts of most other elements, except As, K, and Pb. The amounts of these trace elements are less than  $250 \mu\text{g g}^{-1}$ .

For both products, material with adsorbed P of around  $4.6 \text{ mg P g}^{-1} \text{ DW}$  was used for XRD analysis. Table B.3 shows more details about the 'loaded' material. Figure 5 shows the X-ray diffractogrammes of the untreated, dried, and loaded Phosflow™ and EutroSORB® F. Of the large mode of EutroSORB® F only the untreated diffractogramme is shown.

From the top panel (A), it can be seen that the diffraction patterns of the three treatments of Phosflow™ are visually identical. From the second (B) and third (C) panel, the similarity of untreated Phosflow™ and the small EutroSORB® F mode is striking. The most important difference there, is the peak at around  $29.5^\circ$ , which is only visible in the latter. However, comparison with the crystallography open database (COD), indicates that this can be attributed to the same mineral, böhmite [60]. However, it may also be attributable to calcite.



**Figure 5 – X-ray diffractogrammes** – X-ray diffractogrammes of the products. From top to bottom: A) a comparison of untreated, dried, and loaded Phosflow™; B) untreated Phosflow™; C) the large mode of untreated EutrosORB® F; and a comparison of D) untreated, E) dried, and F) loaded small mode of EutrosORB® F. Counts per second (CPS) is plotted against  $2\theta$ . Database codes from the crystallographic open database (COD) are also indicated [60]. In the lowest three patterns, database peaks at around  $30^\circ$  were cut for convenience.

The large EutrosORB® F mode, in the bottom panels (D-F), differs from both the large EutrosORB® F mode and Phosflow™. According to database comparisons, the large mode consists of calcite [60]. The untreated sample (F) is different from the other two (D, E), including some extra peaks at  $32.5^\circ$ , between  $51^\circ$  and  $53^\circ$ ,  $61.5^\circ$ ,  $68.5^\circ$ , and  $87^\circ$ . The extra peaks may potentially be attributable to lime, based on the diffractogrammes found by Laskar *et al.* [65].

### 3.3 Shaking test

Figure 6 shows the results of the shaking test over time, for each product and every endpoint of interest, along with the linear models for every endpoint. Results of the modelling are shown in Table B.4.

For the ‘Still’ and ‘Weak’ shaking regimes, Eutrosorb® F shows greater mass losses than Phosflow™, as can be seen from the first two pairs of panels in Figure 6. The average  $\Delta M_{\text{shake}}$  and  $\Delta M_{\text{SS}}$  are around 1-2% for Eutrosorb® F, while they are close to 0% for Phosflow™. On the other hand, the average values for these two mass loss endpoints is consistently higher for Phosflow™ in the ‘Strong’ regime, compared to Eutrosorb® F.

The EC shows a somewhat different pattern (third panel pair in Figure 6). Blank samples (40-mL DIW in empty centrifuge tube) yielded water with a median EC of  $3.5 \mu\text{S cm}^{-1}$  (see Table B.1). For Eutrosorb® F, the EC hovers around  $200 \mu\text{S cm}^{-1}$  for all regimes, showing only a light increase over time. The EC in the mixtures with Phosflow™, however, show a visible upward trend over time. The ‘Still’ regime goes from, on average, 178 to  $267 \mu\text{S cm}^{-1}$ , while the other two regimes go from around 300 up to over  $350 \mu\text{S cm}^{-1}$ . These last two regimes, are very similar in terms of the effects on the EC.

Finally, the pH stays approximately constant over time for both products, according to Figure 6. Blank samples (40-mL DIW in empty centrifuge tube) yielded water with a mean pH of  $5.7 \pm 0.5$  (see Table B.1). The effect that Eutrosorb® F has on the mixture’s pH can be characterised as less substantial compared to that of Phosflow™, with the average final pH in all treatments over time sitting between 9.5 and 8.5. Final average pHs in the mixtures with Phosflow™ were between 9.75 and 10.5.

### 3.4 Adsorption kinetics

Figure 7 shows the results from the adsorption kinetics test at room temperature. The upper panel shows the calculated  $Q$ , while the lower panel shows the SRP for the product-treated bottles. Shown alongside these  $Q$  are models using the average model parameters, which Table 5 lists. The ‘High-control’ positive control is associated with Phosflow™ and the ‘Low-control’ positive control is associated with EutrosORB® F. The blanks remain well below  $5 \text{ mg P L}^{-1}$  over the whole experiment. However, most positive controls deviate substantially from the value at  $t = 0$ , sometimes over  $10 \text{ mg P L}^{-1}$ . This is especially true for the ‘High control’ series, which was diluted much more than the ‘Low control’ series (dilution factors of 1430X versus 560X). Consequently,

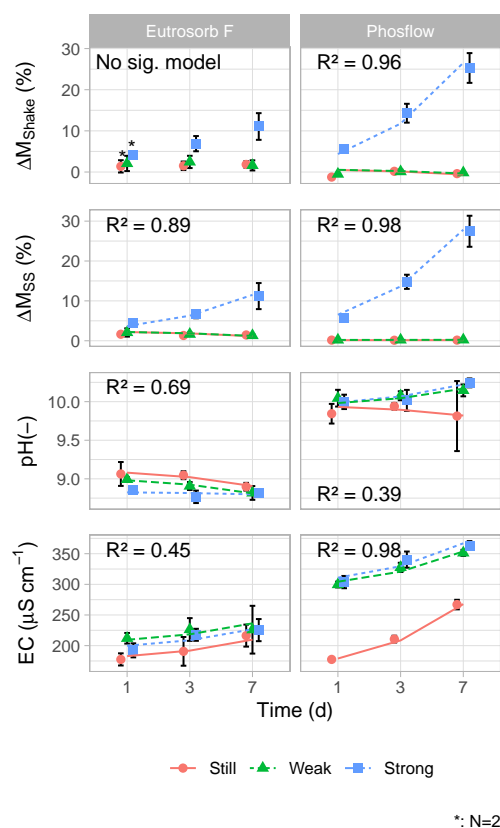


**Figure 6 – Shaking test** – The response of the products Eutrosorb® F and Phosflow™ to physical agitation in deionised water over 7 days. Shown are, from top to bottom, shaking mass loss  $\Delta M_{\text{shake}}$ , suspended solids lost  $\Delta M_{\text{SS}}$ , EC, and pH. Shown are the means with standard deviations, constructed linear models and adjusted  $R^2$ .

the standard deviation can be quite wide at some times during the experiment. Several datapoints with these intervals covering more than  $10 \text{ mg P L}^{-1}$  or  $4 \text{ mg P g}^{-1}$  can readily be spotted among the respective panels of Figure 7. Furthermore, visually, the product-treatments seem to follow the positive controls in their behaviour over time.

The maximum adsorption capacity of Eutrosorb® F,  $9.5 \pm 0.3 \text{ mg P g}^{-1}$ , is within 5% of the value given by their manufacturer,  $10 \text{ mg P g}^{-1}$ ; that of Phosflow™ is lower ( $16 \pm 6$  versus  $26.4 \text{ mg P g}^{-1}$ ), though with the methods employed here, the error is an order of magnitude larger than that associated with Eutrosorb® F. The  $k$  indicate timescales of around  $3.3 \pm 1.4$  and  $16.7 \pm 2.4$  days for Eutrosorb® F and Phosflow™ respectively. Comparing the average model with all data from a given treatment, so across the three replicates, yields a  $R^2$  of 0.79 and 0.42 for the two respective products.

**Table 5 – Adsorption kinetics; mean parameters** – Mean model parameters of pseudo-first-order models of the time series for  $Q$  of each product-treated bottle ( $N = 3$ ). The errors are standard errors of regression.

Parameter	Eutrosorb® F	Phosflow™
$Q_{\text{max}}$ ( $\text{mg P g}^{-1}$ )	$9.5 \pm 0.3$	$16 \pm 6$
$k$ ( $\text{d}^{-1}$ )	$0.30 \pm 0.12$	$0.16 \pm 0.06$

**Table 6 – Adsorption isotherms; fitted Langmuir model** – Parameters in the Langmuir model fitted to the measured  $Q$ -SRP and  $Q$ -TP data. Indicated below the coefficients are standard errors of regression.

Parameter	Eutrosorb® F	Phosflow™
$Q_{\text{max}}$ ( $\text{mg P g}^{-1}$ )	$10.3 \pm 1.4$	$10.3 \pm 1.9$
$K$ ( $\text{L g}^{-1} \text{ P}$ )	$53 \pm 20$	$13^b \pm 10$
$Q_{\text{max,TP}}$ ( $\text{mg P g}^{-1}$ )	$9.0^a \pm 1.2$	$15 \pm 6$
$K_{\text{TP}}$ ( $\text{L g}^{-1} \text{ P}$ )	$66^a \pm 22$	$18^b \pm 14$

a:  $100 \text{ mg P L}^{-1}$  data excluded; b: insignificant ( $p > 0.05$ )

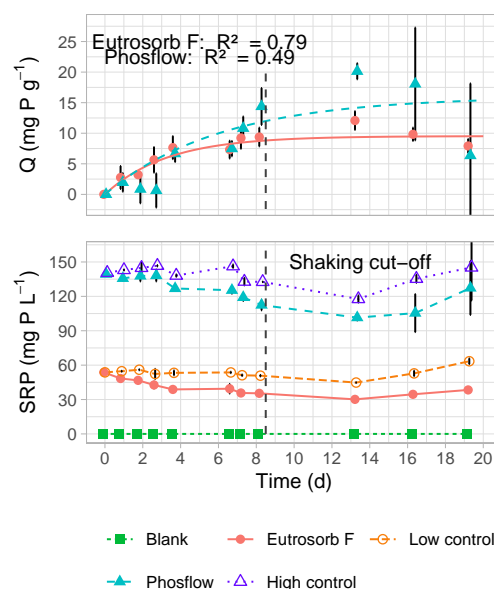


**Figure 7 – Adsorption kinetics** – The upper panel shows mean  $Q$  with respect to  $t = 0$  over time. Curves are models with averaged parameters. The lower panel shows mean SRP over time. 'High control' is the control associated with Phosflow™, while 'Low control' is associated with Eutrosorb® F. The dashed vertical line represents when the bottles were no longer shaken. Errors are standard deviations ( $N = 3$ ).

More detailed results are shown in Figure B.2, which shows  $Q$ , SRP, pH, and  $T$  ( $^{\circ}\text{C}$ ) over time, and Table B.2, which lists individual model parameters.

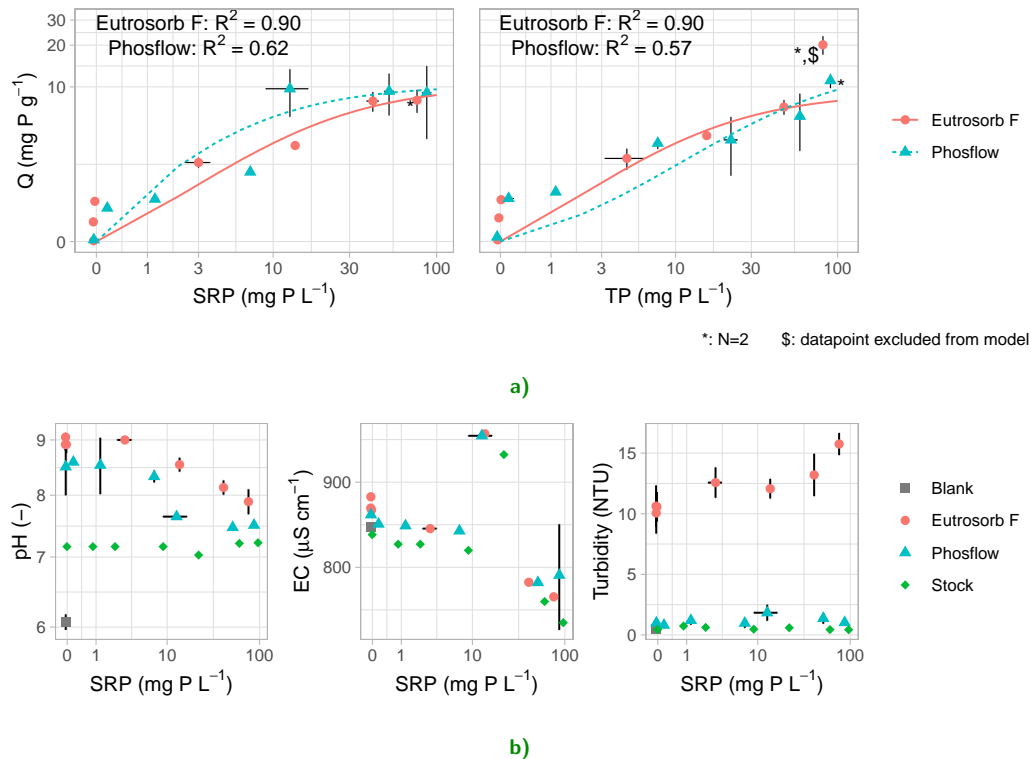


**Figure 8 – Adsorption isotherms & other endpoints** – a)  $Q$  based on the measured SRP or TP versus the measured SRP (left) or TP (right), along with the modelled Langmuir isotherms. b) Means of the other variables measured at the end of the experiment. In the stock solution, they were measured before application of the product. From left to right, the following is shown: pH, EC, and turbidity. All errors are standard deviations ( $N = 3$ , unless indicated otherwise).

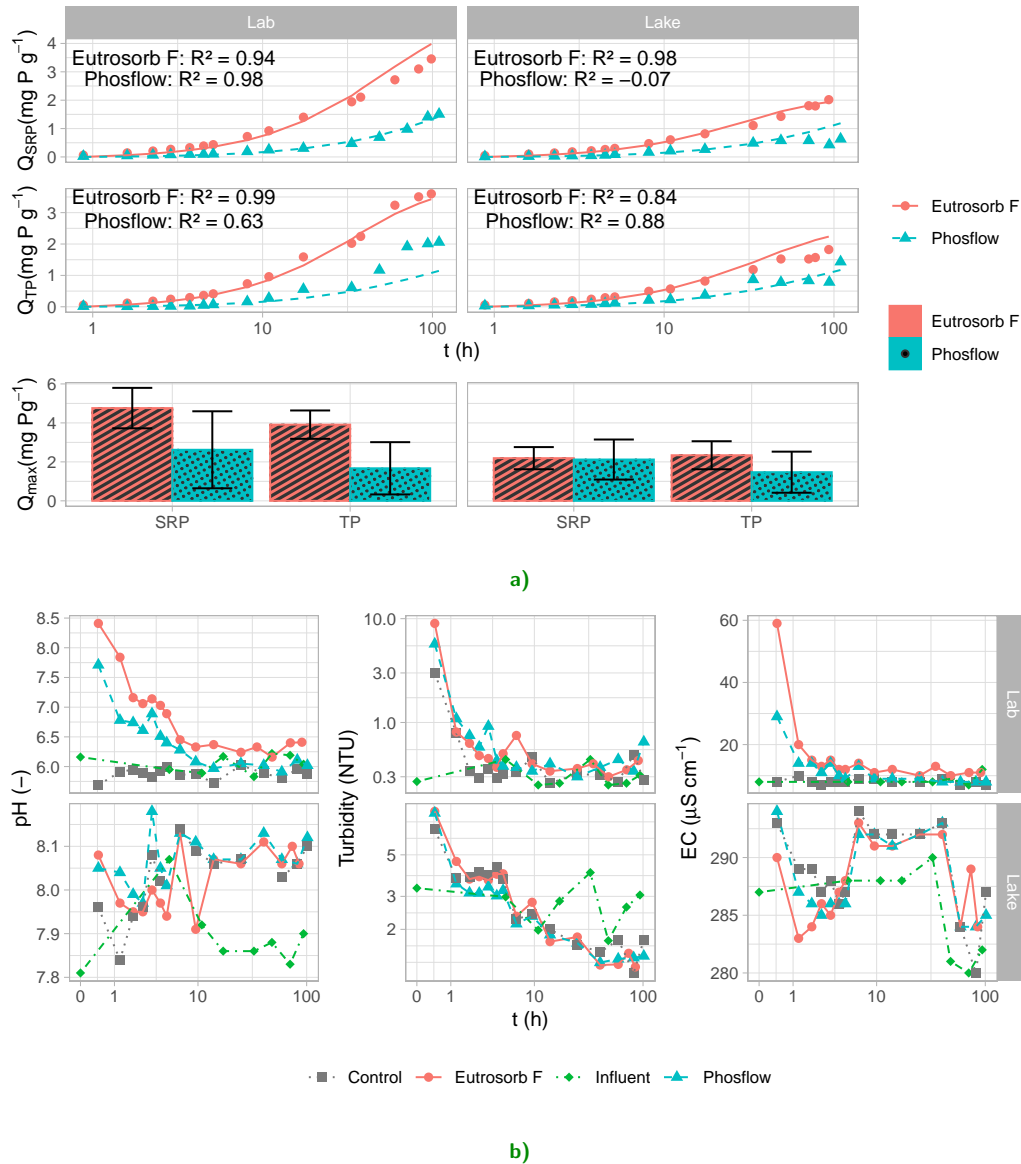
### 3.5 Adsorption isotherms

Figure 8 a) shows the adsorption  $Q$  calculated from the found SRP and TP, versus these same quantities, along with fitted Langmuir isotherms. The parameters of these models are listed in Table 6. For the non-linear least-squares regression on the  $Q$ -TP series of EutrosORB® F the points at around 100 mg P L<sup>-1</sup> were excluded from the fitting data. They had  $Q$  of 22.2 and 18.0 mg P g<sup>-1</sup>, at least a factor 2 larger than all other datapoints of the same series. Their exclusion will be justified in detail in the discussion, but it hinges on the increased turbidity in the mixture.

Generally speaking, all isotherms indicate maximum adsorption capacities of around 10 mg P g<sup>-1</sup> applied product (Table 6). Qualitatively, there seems to be no observable difference between these between these capacities, all lying within one standard error of one another. In fact, the  $Q_{\max}$  found based on SRP removal are the same ( $10.3 \pm 1.4$  for EutrosORB® F and  $10.3 \pm 1.9$  for Phosflow™). One exception to this is the  $15 \pm 6$  mg P g<sup>-1</sup> gained by constructing an isotherm for Phosflow™'s  $Q$ -TP data. Then again, all other capacities lie within its standard error.

The fitted  $K$  seem to indicate that P has a greater affinity for binding to EutrosORB® F rather than to Phosflow™ ( $53 \pm 20$  versus  $13 \pm 10$  L g<sup>-1</sup> P for  $Q$ -SRP and  $66 \pm 22$  versus  $18 \pm 14$  L g<sup>-1</sup> P for  $Q$ -TP). However, the  $K$  recovered for Phosflow™ were not found significant. Correspondingly, the  $R^2$  for Phosflow™'s isotherms is lower than those of EutrosORB® F,  $<0.65$  versus 0.9.

Figure 8 b) shows the other measured variables versus the measured SRP at equilibrium. pH, EC, and turbidity are elevated with respect to the stock solutions in every mixture. pH goes up from the starting value at around 7, up to 8.5 for Phosflow™ and 9 for EutrosORB® F in the batches with lower starting SRP ( $<10$  mg P L<sup>-1</sup>). At higher starting SRP, these changes are smaller, down to 7.5 for Phosflow™ and 8 for EutrosORB® F. For both, EC is elevated by around 25  $\mu\text{S cm}^{-1}$ . However, this can be up to 40 to 50  $\mu\text{S cm}^{-1}$  in EutrosORB® F batches with lower SRP ( $<10$  mg P L<sup>-1</sup>). Turbidity is elevated in Phosflow™ batches, but never beyond 2.5 NTU. In EutrosORB® F batches, values over  $>10$  NTU were recorded, reaching over 15 NTU in batches with an initial SRP of 100 mg P L<sup>-1</sup>.



**Figure 9 – Fixed-bed adsorption** – a) Cumulative adsorbed P for every bed, inferred from experimental SRP and TP (points) and model results (curves). The  $R^2$  compares modelled and experimental cumulative  $Q$ . The lowest panel shows  $Q_{max}$ , according to Equation 11, with calculated standard errors based on linear error propagation. b) Other variables measured in the effluent; from left to right: pH, turbidity, and EC. Note the logarithmic y-axis for turbidity.

### 3.6 Fixed-bed adsorption

The cumulative adsorbed P  $Q$  for the different beds are shown in Figure 9 a), along with estimations of bed MACs  $Q_{max}$ . The models for bed  $Q_{cum,t}$  are much more robust ( $R^2 > 0.8$  for 6 of 8 models) than those of fitted directly to the measured concentrations ( $R^2 < 0.3$  for Phosflow™ and  $0.55 < R^2 < 0.90$  for Eutrosorb® F; see Figure B.3). This is likely because calculating  $Q_{cum,t}$  effectively entails integrating the signal over time.

Eutrosorb® F adsorbs more efficiently under sim-

ilar conditions as Phosflow™, as can be seen from the  $Q$  of the former being consistently higher. Consequently, the calculated MAC is higher for Eutrosorb® F in all 4 cases:  $4.8 \pm 1.1$  versus  $2.6 \pm 2$  and  $2.19 \pm 0.6$  versus  $2.1 \pm 1.1$  mg P g<sup>-1</sup> for SRP-based MACs in lab-based and lake-water-based influents respectively. Note, however, the considerable overlap of the errors estimated via linear error propagation. Both products tend to adsorb less efficiently from the used lake water than from the lab solution. In most cases, the MAC calculated from the SRP-based model somewhat is higher than that from the

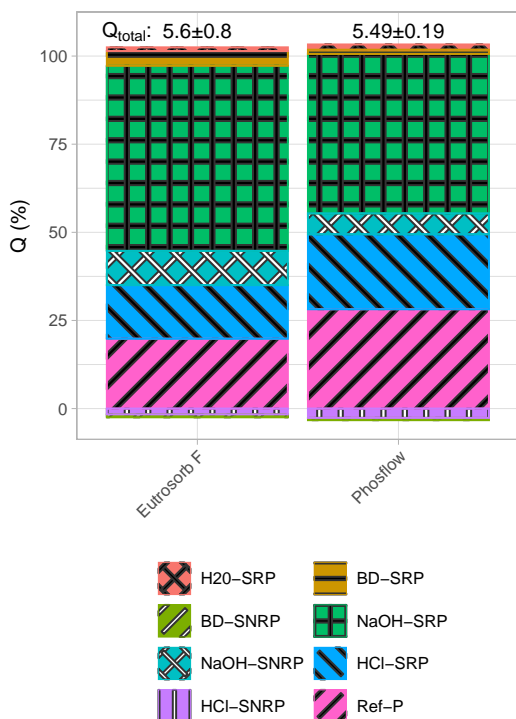


**Figure 10 – Sequential P extraction; relative pools** – Relative size of the 7 different distinguishable P pools in the loaded products. These pools are ordered from top to bottom, starting with phase 1 and ending with phase 5 (see also Table 2). Soluble non-reactive P was gained by subtracting SRP from TP. The values noted  $Q_{total}$  are the mean total adsorbed P in  $\text{mg P g}^{-1}$  with standard deviations.

TP-based model; Eutrosorb® F in lake water seems to be the one exception, though the values are hardly distinguishable, given the estimated errors.

Both products visibly affect different water quality variables in the lab water other than P concentrations, as Figure 9 b) shows. pH is consistently elevated compared to the control, with Eutrosorb® F-treated samples having the highest pH. Over time, this effect decreases in magnitude. The same can be noted of the EC. For turbidity, the picture is a little bit more complicated: the first time step is particularly turbid, with the Eutrosorb® F-treated sample being comparatively very turbid. As time goes on, product-treated beds and the control can hardly be distinguished. For the beds through which lake water was passed, control and products seem largely indistinguishable. Any differences that can be seen are relatively small. It is worth noting that the turbidity decreased over time for both product and control beds.

**Table 7 – Sequential P extraction; Comparisons** – Significantly different groups of products for every fraction when comparing  $Q$  ( $\text{mg P g}^{-1}$ ) across products: empty (E) and loaded (L) Eutrosorb® F and Phosflow™. Thus, each row is one comparison: kruskal-wallis followed by Dunn's test with  $\alpha = 0.05$ . Similar letters indicate homogeneous groupings that cannot be differentiated at the 95% level. Mean  $Q$  with standard deviations are shown in Figure B.4.

Fractions	Eutrosorb® F		Phosflow™	
	E	L	E	L
H2O	a	b	a	b
BD	SRP	ab	c	a
	SNRP	ab	ab	a
NaOH	SRP	ab	c	a
	SNRP	a	b	ac
HCl	SRP	ab	ac	b
	SNRP	ab	ac	b
H2SO4	ab	ac	b	c

### 3.7 Sequential P extraction

Figure 10 shows the mean relative P pools in the loaded products along with their  $Q_{total}$ . The  $Q_{total}$  of the empty Eutrosorb® F and Phosflow™ were  $8 \pm 14$  and  $12 \pm 23 \mu\text{g P g}^{-1}$  respectively, so their relative P-pools are not shown in Figure 10. Noteworthy is the dominance of NaOH-SRP, followed by Ref-P, HCl-SRP, and then NaOH-SNRP. H<sub>2</sub>O-SRP and BD, by contrast, are negligible (<6% combined for both products).

Table 7 gives lettered groups based on pairwise comparisons (Dunn's test) of the different pools in terms of  $Q$  across products (Table B.7 is similar for measured concentrations). Loaded products are functionally indistinguishable. For all dominating pools but one (HCl-SNRP), forming >90% of the total, loaded Phosflow™ is significantly different from its empty counterpart. For Eutrosorb® F, this is not so clear: out of the 4 dominating pools, only NaOH-SRP and NaOH-SNRP are significantly different between the loaded and empty product.

Relative  $Q$  of the loaded products is given in Figure B.5, mean  $Q$  for the different pools across products are given in Figure B.4, and the values for  $Q_{total}$  are given in Table B.6.

## 4 Discussion

The following discussion broadly follows the sub-research questions. First, the physical characteristics and chemical nature of the products are discussed; second, the adsorptive behaviour are discussed in detail; third, expected environmental impacts of product application are hypothesised based on the results and literature. Finally,

these aspects are combined to form a coherent judgement on the fitness-of-purpose of the two products.

#### 4.1 Physical characteristics & chemical nature

The size distributions in Figure 4 show that Phosflow™ is mostly between 4.8 and 2.8 mm in diameter. On the other hand, EutroSORB® F shows a clear 'bimodal' distribution, with the two modes also being visually distinct. Hence, the choice to separate these two fractions for the XRD analysis and aqua regia extraction was deemed justified.

The results of these analysis are found in Figure 5 and Table 4. The small EutroSORB® F mode and Phosflow™ were, as noted, identified as böhmite,  $\gamma$ -AlOOH [60, 66], which is known for its P-adsorbing capabilities [67–70]. Given the determined elemental composition in Table 4, we may then say that the Phosflow™ and the small EutroSORB® F mode contain around 70% böhmite, joined by some substantial but minor amount of Mg- or Ca-based materials. If the existence of pure Mg-minerals is accepted, Phosflow™ contains around 1.5%  $\text{MgCO}_3$  or 0.7% MgO, though none such minerals were observed in the XRD scans (see Figure 5). The Large EutroSORB® F mode, on the other hand, consists almost exclusively of calcite [65, 71], possibly in the form of bivalve shells [72]. However, the presence of lime in the XRD scan of the untreated large mode is notable. On the whole, EutroSORB® F consists of around 40% böhmite and 41% calcite, with the rest being unidentifiable based on these results. Still, other mineral substances with crystalline structure may be largely excluded, such as Fe-(hydr)oxides, clay minerals and other silicates. The same can be said of Phosflow™ regarding the unidentified  $\sim 30\%$ .

With these mineral compositions in mind, we can revisit the LOI in Table 3. Böhmite dehydrates from  $\gamma$ -AlOOH to  $\text{Al}_2\text{O}_3$  when heated in excess of 400 °C [73]. However, given that mass shifted from the large mode to the small mode in Figure 4, it is possible that decarbonation of the calcite contributes to the LOI, potentially causing the large mode to fragment. Important to restate is that the changes in the size distribution are of the same order of that of the error on the mean size fractions, meaning that we should be cautious with drawing conclusions from these changes.

Phosflow™ does not contain sufficient amounts of carbonates to dominate LOI, even though decarbonation could occur with temperatures in excess of 400°C [74]. Other ignitable constituents have not been confirmed, but the related patent application indicates cellulose as a binder, though this was likely mostly burnt off during production [75]. On the other hand, böhmite was

confirmed, so its dehydration is possibly responsible for Phosflow™'s LOI. Given that  $\text{MgCO}_3$  might be present in such small amounts, it is unlikely that it is primarily responsible for the LOI. Thus, the presence of  $\text{MgCO}_3$  over MgO cannot be ascertained.

EutroSORB® F and Phosflow™ are now largely characterised, and further results can be discussed with this context. However, some things are still of note: the found safety data sheet for Phosflow™ indicates  $\text{Al}_2\text{O}_3$  and  $\text{MgCO}_3$  as main ingredients, but this has not been confirmed, contrary to what was hypothesised [47]. The description in a possibly relevant patent could also not be confirmed [75]. The hypothetical composition of EutroSORB® F was more or less confirmed, as it is indeed made of multiple ingredients, one being a known sorbent and another possibly being biogenic. Still, this hypothesis could only be formulated in vague terms, as the relevant patent application was rather unhelpful in providing specific information [48].

The results of the shaking test, shown in Figure 6, show that both products can be mechanically eroded. Phosflow™ is more sensitive to this erosion than EutroSORB® F, though the latter seems to contain small material that can simply be lost by washing. Thus, shaking/stirring at 100 RPM as opposed to 140 RPM was justified for further experiments.

The question arises as to what this means for product application. Above what flow rate or velocity can we expect erosion to take place? A crude order-of-magnitude estimate (appendix A.3) indicates that the maximum average flow rates at 100 and 140 RPM would be around 2 and 2.8  $\text{L min}^{-1}$  respectively. Given that the products erode when shaken at 140 RPM, there is a real risk that the products erode when applied in situations where the flow velocity is between these values and upwards. These are very liberal estimates: smaller figures could be found with proper hydrodynamical modelling or experiments. In the end, the hypothesis of physical stability in water may be accepted, though with some constraints regarding physical abrasion. EutroSORB® F would contribute to turbidity at low flow, but this contribution would be limited, even at higher flow ( $\gtrsim 2 \text{ L min}^{-1}$ ). Noteworthy is the possibility that the background is just the result of initial material that is so small that it can be washed from the rest of the bulk. Thus, this background would be concentrated at the start of application, but would decrease rapidly afterwards. Phosflow™ does not show this background, and should maintain its integrity below  $\sim 2 \text{ L min}^{-1}$ .

#### 4.2 Adsorptive behaviour

The EutroSORB® F's MACs found with the batch and kinetic experiments (see Table 5 and Table 6) agree

with that reported by its producer, at around  $10 \text{ mg P g}^{-1}$  [46]. Phosflow™'s MAC may be between 1.5 and 2.5 times lower than reported by its producer, between 10 and  $15 \text{ mg P g}^{-1}$ , contrary to the initial hypothesis of  $26.3 \text{ mg P g}^{-1}$  [45]. The values found from the adsorption isotherms in Table 6 and the pseudo first-order kinetics models in Table 5 agree, based on their standard errors. However, the adsorption isotherms are likely more reliable, given the large errors in the adsorption kinetics experiment. This variability may be explained by diluting samples with factors of around 1430 and 560 for Phosflow™ and EutroSORB® F respectively.

MACs found via the fixed-bed experiment in Figure 9 a) were a factor 4 lower compared to the other found MACs, except that of EutroSORB® F in lab solution, which was a factor 2 lower. In a review of edge-of-field P filter materials, Mendes *et al.* [39] state that hydraulic properties and retention time are crucial factors in the effectiveness of a fixed-bed P adsorbent. Whether using larger beds could increase the fixed-bed MAC, then, depends on whether the small beds used here were representative of the bulk, hydraulically speaking. If not, MACs could be increased by using larger beds.

Broadly speaking, SRP has shown a greater affinity for EutroSORB® F, rather than Phosflow™. This can be seen from the faster adsorption in the adsorption kinetics experiment Figure 7 with a smaller  $k$  in Table 5, the greater  $K$  of the Langmuir isotherms in Table 6, and the greater removal during the fixed-bed experiment in Figure 9 a) (and larger  $k_B$  in Table B.5).

With all of that in mind, one may explore how the performance of the products compares to literature. Böhmite, an Al-oxyhydroxide, is part of class of minerals known for their adsorbing capabilities. It may have an MAC anywhere between 11.7 and  $32.6 \text{ mg P g}^{-1}$ , depending on conditions such as pH, temperature, and specific surface area [68, 76, 77]. The negative pH-dependence of anion adsorption is typical of Al-oxyhydroxides [78]. Affinity for adsorption is decreased in the presence of humic acids [76], which may directly explain the reduced adsorption in the lake-water fixed-bed setup, compared to the lab solution.

Calcite too, can have a wide range of MACs, depending on experimental conditions. Both 31 [79] and  $0.13 \text{ mg P g}^{-1}$  [80] have been reported, differing in experimental conditions and specific surface area. With regards to Mg-based sorbents, MACs can be quite high for products with Mg-contents upwards of 10%. Sorbents meant for industrial-scale P-removal in wastewater treatment can be optimised to MACs from 6 to well over  $100 \text{ mg P g}^{-1}$  product [81]. For both calcite and MgO or  $\text{MgCO}_3$ , increasing pH should result in crystallisation of insoluble mineral species, like hydroxyapatite and struvite (in the presence of ammonium) [79, 81].

When comparing the MAC of the tested products, they are similar to those of the following solid-state P-sorbents: half-burned dolomite, La-modified bentonite, Al-, Fe-, and Al/Fe-modified bentonite (based on a list compiled by Lürling *et al.* [24]). As described by Douglas *et al.* [40], all of them contain Al, Fe, La, carbonates, or some combination, like Phosflow™ and EutroSORB® F. A notable difference is that most of these are modified clay minerals (bentonite specifically), while Phosflow™ and EutroSORB® F are not.

Now we know what the products are and what we may expect from them in terms of general performance, but we can also make some observations regarding how P is distributed within them. From the results of the sequential P extraction in Figure 10, it is clear that the pool extractable by NaOH dominates the rest, for both products. This should mean that Al- or Mn-(oxyhydr)oxides dominate the adsorption processes in the products. Since no Mn-based minerals were found in XRD analysis, one may consider the Al-based minerals as the dominant adsorbing ingredient in absolute terms. These minerals are typically known for adsorbing oxyanions via electrostatic interactions and ligand exchange, forming inner-sphere complexes [70, 78]. The lack of crystalline bonds with P in the diffractogrammes indicate that only these surface complexations occurred. However, the substantial contributions of the HCl and  $\text{H}_2\text{SO}_4$  extractions show that carbonates and mineral formation should play an appreciable role, even an outsized one for Phosflow™. Surface complexation onto calcite was deemed to be dominant at low SRP ( $<50 \text{ } \mu\text{g P L}^{-1}$ ) by Flower *et al.* [80], and Ekamparam & Singh [82] observed the formation of apatite-species, as did Wan *et al.* [83]. As a result, the formation of such minerals should have been possible in EutroSORB® F.

Mg-based phosphate mineral formation was likely not possible in the adsorption kinetics experiment, as a precipitation experiment by Tamimi *et al.* [84] indicates. Furthermore, the review by Silva & Baltrusaitis [81] notes that surface complexation is the typical mechanism for P-removal by Mg-minerals, with later mineralisation in combination with ammonium as struvite ( $\text{MgNH}_4\text{PO}_4 \cdot 6\text{H}_2\text{O}$ ) as a final endpoint. This may be understood to be contrary to what was visible in Figure 10, as one should expect this mineralisation to be much more limited given the supposed dominance of surface complexation.

The absence of P-based minerals in the XRD scans (see Figure 5) is noteworthy, particularly for EutroSORB® F. Presumably, the around 2.5% by mass that, e.g., hydroxy-apatite would form of the calcite bulk would be too small to be observable against the background in the XRD patterns. Typical molar ratios of Ca:P used in literature upon apatite-synthesis seem to be larger than what was used here ( $>0.5$  versus  $<0.2$ )

[80, 82, 83]. As such, it is difficult to say whether these minerals should have been visible or not. An analogous argument can be made for the Mg in Phosflow™.

Thus, with regards to P-mineral formation, we are left with an obscured picture for EutroSORB® F and with a paradox for Phosflow™. After, all, the results indicate that mineralisation took place, but there is no known constituent of Phosflow™ that can be expected to bring this about to an appreciable degree. This paradox could be resolved by considering that the P was adsorbed to surfaces deep within the pellets. If the porosity is high enough, but the permeability sufficiently limited, the extractants may not have been able to properly access the P over the short shaking periods.

Another problem is that the total extracted P is conspicuously lower than what might have been expected from the kinetics experiment, 5.6 and 5.19 mg P g<sup>-1</sup> versus closer to 10 mg P g<sup>-1</sup> (see Figure 10 and Figure 7). Of course, the loaded products were dried between that experiment and extraction. Potentially, the adsorbing capacity or affinity of the products decreased with temperature, thereby releasing P, which could then form evaporite solids. This is possible, though the adsorbing capabilities of dominant mineral böhmite seem dependent on further experimental conditions. Some reported that  $Q_{\max}$  decreased with temperature [67, 77], though another found the opposite [68]. Not to mention that these evaporites would have been visible in the diffractogrammes. Still, overestimated  $Q_{\max}$  from the kinetics results seems unlikely, given its agreement with the adsorption isotherms. Thus, there is another solution that could resolve the Mg-P mineral paradox from before: the used extractants may not have been able to fully desorb the P. The leftovers would be moved on to the next extraction phase, and by the end some amount of P would simply be missed and left in the products. Causes for this could be that the extraction volumes were too small, the extraction times too short, or indeed that the products were not permeable enough to access the internal surfaces. If this line of thinking is true, then the quantitative results of the sequential extraction after phase 2 with the BD-reagent cannot be trusted.

Which sequence of events is correct cannot be determined from the results presented here. For now, the prevalence of Al-bound P is clear in both products, and P-mineralisation to calcite is possible in EutroSORB® F. The mechanism governing the distribution of P in the strongly-bound fractions in Phosflow™ is still an open question, however. The presented results give indications that are contradictory to literature.

### Limitations of the adsorption experiments

It is necessary to point out some limitations to the findings of the other adsorption experiments, beyond what has already been mentioned. To start: two datapoints for the  $Q$ -TP relation of EutroSORB® F in Figure 8 a) were excluded from the isotherm, which barred model convergence when included. Turbidity in the EutroSORB® F mixtures increased with measured SRP (see Figure 8 b)), from around 10 to around 15.7. The samples at 100 mg P L<sup>-1</sup> were the extreme. Given that the found  $Q$  was much higher than is deemed reasonable, the interference could not be a result of light scattering off colloidal material, increasing the TP-signal [85]. Rather, adsorbent colloidal may have formed a complexation surface during analysis [86]. Given that the  $Q$  calculated from SRP was much more in line with expectations, it is reasonable to consider that this complexation did not take place before analysis. In the end, TP would be reduced due to this interference, leading to anomalously high  $Q$ , which should be excluded from the TP-based isotherm.

A second pertinent point, is that in every adsorption experiment, the goodness-of-fit of regressed models is poorer for Phosflow™ than for EutroSORB® F. In the adsorption rate curve, this may be attributed to the large uncertainties in the measured SRP.

For the adsorption isotherms, however, invalidity of the assumptions underpinning the Langmuir model seems plausible. The main suspect assumption is that of homogeneous sites within the sorbent [69]. After all, the results from the sequential extraction indicate that this assumption cannot really be assumed to hold, for neither product. There may have been several different inactivation processes at play (as long as validity of the sequential P extraction results may be assumed). Furthermore, precipitation of apatites may strictly not even be called 'adsorption'. As such, the Langmuir isotherms used and found here should be interpreted as empirical approximations of a more complicated situation.

This trend of poor fit extends to the breakthrough curves. Although the weak time-dependence may be one culprit of the weak fit, the inconsistent flow rate, and thereby less smooth adsorption efficiency, must also have played a role. The actual time-dependence might then simply have been overshadowed by this extra variability. The integrative nature of the  $Q$ -curve in Figure 9 a) smooths out some of this variability. Thus, a sufficient goodness-of-fit ( $R^2 > 0.5$ ) would still indicate that some time-dependence is captured in the breakthrough curves, and therefore that adsorption is taking place. Indeed, this seems to be the case, except for the SRP-based  $Q$ -curve with lake-water influent. Potentially, this may point to P being adsorbed to suspended material.

### 4.3 Environmental impact

Both products seem to have substantial pH-buffering capacity: they substantially elevate the pH of DIW, as shown in Figure 6 (but also Figure B.2 b), Figure 8 b), and Figure 9 b)). Phosflow™ increases pH to around 10, and EutroSORB® to around 8.8 in the shaking test. EC is also elevated in these systems. Under the used experimental conditions and outcomes ( $\text{pH} > 7.5$ ), aluminium minerals should be more soluble than calcium carbonate [87, 88]. Thus, one would consider the elevated EC and pH mostly a result of its dissolution or dissociation. The matter of interest, then, is whether this buffering capacity will meaningfully impact the pH of the water the products are applied in. The lake-water-based fixed-bed experiment indicates that such an effect would be minor ( $\Delta\text{pH} < 0.3$ ; see Figure 9 b)).

Both products release suspended material, the degree of which is dependent on the flow regime, but also the size distribution of the products themselves. The fixed-bed experiment with lab-influent also shows elevated turbidity, but the initial drop in this increase is very steep, so overall effects may be very limited in the grand scheme of things. Drawing further parallels between the shaking test and turbidity measurements elsewhere is not sound because the relation between turbidity and suspended solids was not quantified [89].

The effects on the lake-water used in the fixed-bed adsorption experiment, as shown in the lower panels of Figure 9 b), are negligible. This goes for pH and EC, while the turbidity decreased over time for all three treatments. Regarding the latter, potentially solids got trapped in the tubes, diminishingly accumulating there.

The product constituents are, in principle, not out of place in the environment. Hence, although Al poses a toxicity risk at the fringes of environmental pH [90, 91], there is no reason to believe that the products should pose a toxicological threat to aquatic systems [92]. At least, not in applications where there is limited overall impact on pH ( $\lesssim 9$ ) and EC, and thereby bioavailability, such as in the lake-water based fixed-bed experiment. Under high-pH conditions ( $\text{pH} > 9$ ), Al-minerals may dissolve, thereby releasing the toxic  $\text{Al}(\text{OH})_4^-$  into solution [92]. Excessive physical abrasion may cause Phosflow™ to release more bioavailable material under such high-pH conditions, if EC in Figure 6 may be taken as a proxy of general release of ions. A similar argument can be made for EutroSORB® F, though the effect of abrasive action is less clear.

It is also instructive to make a cursory comparison of the contents of the other analysed metals to surveys of metal contents in soils. Whether using the products should form an additional source compared to the soils around it may then be hypothesised, statistical models

of Europe, by Lado *et al.* [93] and Tóth *et al.* [94] can be used for this purpose. The former indicates that this is not the case for As, Cd, Cr, Cu, Ni, Pb, and Zn [93]. That is to say, the values in Table 4 are on the far lower end of what those maps indicate. The latter indicates the same thing for As, Cd, Cr, Cu, Mn, Ni, and Pb [94]. Thus, one need not expect that potentially toxic trace elements in the products pose an extra ecotoxicological hazard under moderate conditions ( $6 < \text{pH} < 8$ , DOC present, etc.).

### 4.4 Fit for purpose?

Given all the above, a general judgement of the fitness for purpose of the two products is in order. Table 8 gives an overview of the found MACs based on SRP removal.

Phosflow™ should be considered physically stable under low-flow conditions, with a likely limited effect on the pH, EC, and turbidity of environmental waters when used in a fixed-bed capacity. However, its greater sensitivity to physical abrasion should make water managers cautious when using it under higher-flow conditions ( $> 2 \text{ L min}^{-1}$ ), and may release more bioavailable material under such conditions. It has a static SRP MAC at equilibrium of around  $10.3 \text{ mg P g}^{-1}$ , so it is capable of substantial P adsorption. However, the fixed-bed SRP MAC found from the lake-water-based Bohart-Adams model is much lower, around  $2.1 \text{ mg P g}^{-1}$ .

EutroSORB® F is more stable than Phosflow™, has a smaller effect on pH and EC, but does release some amount of material upon first application. It is, however, less sensitive to physical abrasion. Its static SRP MAC at equilibrium is very similar to that of Phosflow™, at around  $10.3 \text{ mg P g}^{-1}$ . Again, fixed-bed SRP MACs were lower than this static value,  $4.8$  and  $2.2 \text{ mg P g}^{-1}$  for the tests with lab-based and lake-water-based influents respectively. Here, the reduction that takes place with the more 'natural' water is apparent, and could be caused by all sorts of confounding factors, like particulate OM or DOC, among others.

The Bohart-Adams models for lake-water-based influents can be used to estimate product lifetimes under more realistic conditions ( $2 \text{ kg product}$ ,  $0.5 \text{ mg P L}^{-1}$ ; see Figure B.6), thereby taking these confounding factors into account. The products would have a lifetime of several weeks in low-flow conditions ( $0.2 \text{ L min}^{-1}$ ), but neither would last longer than 20 days in more realistic baseflow conditions ( $2 \text{ L min}^{-1}$ ). However, these estimates are quite untrustworthy, given that for both products one parameter was found insignificant when fitting the breakthrough curves (see Table B.5). This is especially true for Phosflow™, for which the time-dependence was insignificant.

Product performance may therefore in the end be

**Table 8 – Found MACs** – The  $Q_{\max}$  based on SRP removal found for EutroSORB® F and Phosflow™ by the experiments reported here, along with the values reported by SePRO Co. and Water Warriors Inc.. From top to bottom, they come from the pseudo-first-order models fitted to the kinetics data, the found Langmuir isotherms, the Lab-based Bohart-Adams model, and the Lake-water-based Bohart-Adams model.

$Q_{\max}$ (mg P g <sup>-1</sup> )	EutroSORB® F	Phosflow™
Hypothesis	~10 [46]	26.4 [45]
PFO	9.5 ± 0.3	16 ± 6
Langmuir	10.3 ± 1.4	10.3 ± 1.9
BA, Lab	4.8 ± 1	2.6 ± 2
BA, Lake	2.2 ± 0.6	2.1 ± 1

said to be quite dependent on the environmental context in which the products are applied. In turn, the response to this context is a function of the composition of the products and how they adsorb the P. In both products P adsorption is dominated by an Al-oxyhydroxide, onto which surface complexation may be assumed. In EutroSORB® F, the mineralisation of P into Ca-based apatites may be deemed possible. However, what causes a majority of the P to be 'precipitated' in Phosflow™ is unclear. With all that in mind, one could expect that P adsorbed to either product is, generally, not readily bioavailable at moderate pH. However, users should be cautious of high-pH (pH > 9) conditions; böhmite P-sorption capacity reduces with increasing pH, with a point of zero charge between pH 8.5 and 9.5 [68, 70, 77, 78]. Furthermore, under such conditions it would start dissolving, releasing toxic Al(OH)<sub>4</sub><sup>-</sup> in the process [92].

## 5 Conclusions & Outlook

Here, Phosflow™ and EutroSORB® F were tested in various ways to determine whether they are fit for purpose as in-stream P-adsorbents. EutroSORB® F contains around 40% böhmite and around 41% calcite by mass. Phosflow™ contains around 71% percent böhmite by mass, along with some 4.3 mg Mg g<sup>-1</sup>.

One should take care that flow conditions do not exceed what the products can handle: between 5.8 and 8.2 cm s<sup>-1</sup> and upwards the products may erode and release suspended solids or constituent material into the environment. In particular, aluminium or aluminium minerals, like the main constituent böhmite, would be released. Though the products can increase pH and EC in unbuffered systems, the lake-water-based fixed experiment indicates that such effects should be minor in more natural, and therefore more extensively buffered, systems. Thus, the products should not be expected to pose an ecotoxicological hazard at moderate pH (< 9),

though under more extreme conditions, toxic dissolved Al-species could be released. With static equilibrium MACs around 10.3 mg P g<sup>-1</sup>, both products are fairly efficient P-sorbents. However, MACs can be reduced by a factor of around 5 when the products are applied in a fixed-bed experiment with lake-water-based influent.

This report provides the basis for future testing of both products by investigating what the products are made of and what might be expected of them when applied in the field. A cost-benefit analysis was beyond the scope of this research, but is still necessary, given that the price per captured kg P is still not known. Moreover, it would have to be applied all across a (sub-)catchment, and it is by no means clear whether that is more cost-effective than regularly applying in-lake measures. Finally, upscaled fixed-bed testing should be done with environmental water, in which varying pH and flow conditions would be crucial. Effluents should then also be analysed for dissolved Al-species. With such testing, toxicological hazards and risks may not just be hypothesised, but quantified, as well as product lifetimes and performance in the field determined.

## Declaration of competing interest

The author has no relevant financial interest to declare.

There has been close correspondence with Dr B.C. Fuhrmann and Dr K.E. Waters-Hart with regarding the project (see e.g. Appendix C.1). Dr Fuhrmann co-developed EutroSORB® F at EutroPHIX, a subsidiary of SePRO Co.. He provided feedback to the penultimate version of this report. Dr Waters-Hart was employed as a group manager for aquatic science at Phoslock Environmental Technologies, which had the rights to distribute Phosflow™.

## Acknowledgements

I would like to thank my supervisors for their time and guidance; I have learnt a lot from them, as well as the work I did under their supervision. I am grateful to the lab technicians at AEW for their invaluable practical know-how and support. My thanks also go out to the WUR soil chemistry laboratory and Ilse Gerrits from the Environmental Technology chair group, who carried out the aqua regia extraction followed by ICP-MS/OES and XRD analysis respectively. I appreciate Dr. Byran Fuhrmann and Dr. Kate Waters-Hart for their interest and input into this project, as well as my colleague Wieneke Savonije; the insights they provided and the discussions we had were very valuable. Finally, I would like to thank everyone else at the AEW chair group for the open and friendly atmosphere.

## References

1. Craig, L. S. *et al.* Meeting the Challenge of Interacting Threats in Freshwater Ecosystems: A Call to Scientists and Managers. *Elementa: Science of the Anthropocene* **5** (eds Zak, D. R. & Groffman, P. M.) 72. doi:10.1525/elementa.256 (2017).
2. Albert, J. S. *et al.* Scientists' Warning to Humanity on the Freshwater Biodiversity Crisis. *Ambio* **50**, 85–94. doi:10.1007/s13280-020-01318-8 (2021).
3. Dudgeon, D. Multiple Threats Imperil Freshwater Biodiversity in the Anthropocene. *Current Biology* **29**, R960–R967. doi:10.1016/j.cub.2019.08.002 (2019).
4. Huisman, J. *et al.* Cyanobacterial Blooms. *Nature Reviews Microbiology* **2018 16:8 16**, 471–483. doi:10.1038/s41579-018-0040-1 (2018).
5. Heino, J. *et al.* Lakes in the Era of Global Change: Moving beyond Single-Lake Thinking in Maintaining Biodiversity and Ecosystem Services. *Biological Reviews* **96**, 89–106. doi:10.1111/brv.12647 (2021).
6. Hou, X. *et al.* Global Mapping Reveals Increase in Lacustrine Algal Blooms over the Past Decade. *Nature Geoscience* **2022 15:2 15**, 130–134. doi:10.1038/s41561-021-00887-x (2022).
7. Smith, V. H. Eutrophication of Freshwater and Coastal Marine Ecosystems A Global Problem. *Environmental Science and Pollution Research* **10**, 126–139. doi:10.1065/esor2002.12.142 (2003).
8. Le Moal, M. *et al.* Eutrophication: A New Wine in an Old Bottle? *Science of The Total Environment* **651**, 1–11. doi:10.1016/j.scitotenv.2018.09.139 (2019).
9. Scheffer, M., Hosper, S. H., Meijer, M. L., Moss, B. & Jeppesen, E. Alternative Equilibria in Shallow Lakes. *Trends in Ecology & Evolution* **8**, 275–279. doi:10.1016/0169-5347(93)90254-M (1993).
10. Wetzel, R. G. in *Limnology (Third Edition)* (ed Wetzel, R. G.) Third Edition, 129–150 (Academic Press, San Diego, 2001). doi:10.1016/B978-0-08-057439-4.50012-5.
11. Anderson, D. M., Gilbert, P. M. & Burkholder, J. M. Harmful Algal Blooms and Eutrophication Nutrient Sources, Composition, and Consequences. *Estuaries* **25**, 704–726. doi:10.1007/BF02804901 (2002).
12. Stackpoole, S. M., Stets, E. G. & Sprague, L. A. Variable Impacts of Contemporary versus Legacy Agricultural Phosphorus on US River Water Quality. **116**, 20562–20567. doi:10.5066/P972DHYF (2019).
13. Häder, D.-P. *et al.* Anthropogenic Pollution of Aquatic Ecosystems: Emerging Problems with Global Implications. *Science of The Total Environment* **713**, 136586. doi:10.1016/j.scitotenv.2020.136586 (2020).
14. Chen, Y., Destouni, G., Goldenberg, R. & Prieto, C. Nutrient Source Attribution: Quantitative Typology Distinction of Active and Legacy Source Contributions to Waterborne Loads. *Hydrological Processes* **35**. doi:10.1002/hyp.14284 (2021).
15. McCrackin, M. L. *et al.* A Century of Legacy Phosphorus Dynamics in a Large Drainage Basin. *Global Biogeochemical Cycles* **32**, 1107–1122. doi:10.1029/2018GB005914 (2018).
16. Wetzel, R. G. in *Limnology (Third Edition)* (ed Wetzel, R. G.) Third Edition, 239–288 (Academic Press, San Diego, 2001). doi:10.1016/B978-0-08-057439-4.50017-4.
17. Wetzel, R. G. in *Limnology (Third Edition)* (ed Wetzel, R. G.) Third Edition, 205–237 (Academic Press, San Diego, 2001). doi:10.1016/B978-0-08-057439-4.50016-2.
18. Horppila, J. Sediment Nutrients, Ecological Status and Restoration of Lakes. *Water Research* **160**, 206–208. doi:10.1016/j.watres.2019.05.074 (2019).
19. Kang, L. *et al.* Bloom-Induced Internal Release Controlling Phosphorus Dynamics in Large Shallow Eutrophic Lake Taihu, China. *Environmental Research* **231**, 116251. doi:10.1016/J.ENVRES.2023.116251 (2023).
20. Ji, N., Liu, Y., Wang, S., Wu, Z. & Li, H. Buffering Effect of Suspended Particulate Matter on Phosphorus Cycling during Transport from Rivers to Lakes. *Water Research* **216**. doi:10.1016/j.watres.2022.118350 (2022).
21. Bin Zhang, Z., bo Tan, X., lei Wei, L., miao Yu, S. & ji Wu, D. Comparison between the Lower Nansi Lake and Its Inflow Rivers in Sedimentary Phosphorus Fractions and Phosphorus Adsorption Characteristics. *Environmental Earth Sciences* **66**, 1569–1576. doi:10.1007/s12665-011-1400-6 (2012).
22. Paerl, H. W. *et al.* Mitigating Eutrophication and Toxic Cyanobacterial Blooms in Large Lakes: The Evolution of a Dual Nutrient (N and P) Reduction Paradigm. *Hydrobiologia* **847**, 4359–4375. doi:10.1007/s10750-019-04087-y (2020).
23. Abell, J. M., Özkundakci, D., Hamilton, D. P. & Reeves, P. Restoring Shallow Lakes Impaired by Eutrophication: Approaches, Outcomes, and Challenges. *Critical Reviews in Environmental Science and Technology* **52**, 1199–1246. doi:10.1080/10643389.2020.1854564 (2022).
24. Lüring, M., Mackay, E., Reitzel, K. & Spears, B. M. Editorial – A Critical Perspective on Geo-Engineering for Eutrophication Management in Lakes. *Water Research* **97**, 1–10. doi:10.1016/j.watres.2016.03.035 (2016).
25. Augustyniak-Tunowska, R. *et al.* Characteristics of P Adsorption by Profundal Bottom Deposits of Kortowskie Lake (Poland), Restored by the Hypolimnetic Withdrawal Method. *Applied Sciences (Switzerland)* **13**. doi:10.3390/app13031861 (2023).
26. Bormans, M., Maršálek, B. & Jančula, D. Controlling Internal Phosphorus Loading in Lakes by Physical Methods to Reduce Cyanobacterial Blooms: A Review. *Aquatic Ecology* **50**, 407–422. doi:10.1007/s10452-015-9564-x (2016).
27. Hamilton, D. P., Salmaso, N. & Paerl, H. W. Mitigating Harmful Cyanobacterial Blooms: Strategies for Control of Nitrogen and Phosphorus Loads. *Aquatic Ecology* **50**, 351–366. doi:10.1007/s10452-016-9594-z (2016).
28. Triest, L., Stiers, I. & Van Onsem, S. Biomanipulation as a Nature-Based Solution to Reduce Cyanobacterial Blooms. *Aquatic Ecology* **50**, 461–483. doi:10.1007/s10452-015-9548-x (2016).
29. Kotta, J. *et al.* Cleaning up Seas Using Blue Growth Initiatives: Mussel Farming for Eutrophication Control in the Baltic Sea. *Science of The Total Environment* **709**, 136144. doi:10.1016/J.SCITOTENV.2019.136144 (2020).
30. Gao, H. *et al.* Combined Effects of Submerged Macrophytes and Aquatic Animals on the Restoration of a Eutrophic Water Body—A Case Study of Gonghu Bay, Lake Taihu. *Ecological Engineering* **102**, 15–23. doi:10.1016/J.ECOLENG.2017.01.013 (2017).
31. Withers, P. J. A. & Jarvis, S. C. Mitigation Options for Diffuse Phosphorus Loss to Water. *Soil Use and Management* **14**, 186–192. doi:10.1111/j.1475-2743.1998.tb00638.x (1998).

32. Kuster, A. C., Pilgrim, K. M., Kuster, A. T. & Huser, B. J. Field Application of Spent Lime Water Treatment Residual for the Removal of Phosphorus and Other Pollutants in Urban Stormwater Runoff. *Water (Switzerland)* **14**. doi:10.3390/w14132135 (2022).
33. Penn, C. J., McGrath, J. M., Rounds, E., Fox, G. & Heeren, D. Trapping Phosphorus in Runoff with a Phosphorus Removal Structure. *Journal of Environmental Quality* **41**, 672–679. doi:10.2134/jeq2011.0045 (2012).
34. Penn, C. J. The Past, Present, and Future of Phosphorus Removal Structures. *Water* **13**, 797. doi:10.3390/w13060797 (2021).
35. Jeppesen, E. et al. Lake Responses to Reduced Nutrient Loading - An Analysis of Contemporary Long-Term Data from 35 Case Studies. *Freshwater Biology* **50**, 1747–1771. doi:10.1111/j.1365-2427.2005.01415.x (2005).
36. Hoffmann, C. C. et al. An Overview of Nutrient Transport Mitigation Measures for Improvement of Water Quality in Denmark. *Ecological Engineering* **155**, 105863. doi:10.1016/J.ECOLENG.2020.105863 (2020).
37. Heal, K. V. et al. Enhancing Phosphorus Removal in Constructed Wetlands with Ochre from Mine Drainage Treatment. *Water Science & Technology* **51**, 275–282. <http://iwaponline.com/wst/article-pdf/51/9/275/434797/275.pdf> (2005).
38. Groenenberg, J. E., Chardon, W. J. & Koopmans, G. F. Reducing Phosphorus Loading of Surface Water Using Iron-Coated Sand. *Journal of Environmental Quality* **42**, 250–259. doi:10.2134/jeq2012.0344 (2013).
39. Mendes, L. R. D., Pugliese, L., Canga, E., Wu, S. & Heckrath, G. J. Analysis of Reactive Phosphorus Treatment by Filter Materials at the Edge of Tile-Drained Agricultural Catchments: A Global View of the Current Status and Challenges. *Journal of Environmental Management* **324**, 116329. doi:10.1016/j.jenvman.2022.116329 (2022).
40. Douglas, G. B. et al. Guiding Principles for the Development and Application of Solid-Phase Phosphorus Adsorbents for Freshwater Ecosystems. *Aquatic Ecology* **50**, 385–405. doi:10.1007/s10452-016-9575-2 (2016).
41. Lüring, M. & Mucci, M. Mitigating Eutrophication Nuisance: In-Lake Measures Are Becoming Inevitable in Eutrophic Waters in the Netherlands. *Hydrobiologia* **847**, 4447–4467. doi:10.1007/s10750-020-04297-9 (2020).
42. Noyma, N. P. et al. Coagulant plus Ballast Technique Provides a Rapid Mitigation of Cyanobacterial Nuisance. *PLOS ONE* **12** (ed Singer, A. C.) e0178976. doi:10.1371/journal.pone.0178976 (2017).
43. Qin, B. et al. Water Depth Underpins the Relative Roles and Fates of Nitrogen and Phosphorus in Lakes. *Environmental Science & Technology* **54**, 3191–3198. doi:10.1021/acs.est.9b05858 (2020).
44. Huser, B. J., Futter, M., Lee, J. T. & Perniel, M. In-Lake Measures for Phosphorus Control: The Most Feasible and Cost-Effective Solution for Long-Term Management of Water Quality in Urban Lakes. *Water Research* **97**, 142–152. doi:10.1016/j.watres.2015.07.036 (2016).
45. Phosflow <https://www.waterwarriorsinc.com/phosflow> (2023).
46. EutroSORB F | Phosphorus Filtration Technology <https://eutrosorb.com/eutrosorb-f.html> (2023).
47. Phosflow Pellets Safety Data Sheet 2022. <https://www.petwatersolutions.com/wp-content/uploads/2022/12/Phosflow-SDS-NZ-August-2022.pdf> (2023).
48. Fuhrmann, B. C., Bishop, W. M., Armel, G. R. & Spinelli, K. M. US20220289602A1. <https://patents.google.com/patent/US20220289602A1/en> (2023)(2022).
49. Pan, M. et al. Synergistic Recapturing of External and Internal Phosphorus for in Situ Eutrophication Mitigation. *Water (Switzerland)* **12**. doi:10.3390/w12010002 (2020).
50. R Core Team. *R: A Language and Environment for Statistical Computing* R Foundation for Statistical Computing (Vienna, Austria, 2023). <https://www.R-project.org/>.
51. NNI. *Water: Photometric Determination of the Content of Dissolved Orthophosphate and Total Content of Phosphorus Compounds by Continuous Flow Analysis* 1986.
52. Wickham, H. *ggplot2: Elegant Graphics for Data Analysis* <https://ggplot2.tidyverse.org> (Springer-Verlag New York, 2016).
53. Kassambara, A. *ggpubr: 'ggplot2' Based Publication Ready Plots* R package version 0.6.0 (2023). <https://CRAN.R-project.org/package=ggpubr>.
54. Pedersen, T. L. *patchwork: The Composer of Plots* R package version 1.1.3 (2023). <https://CRAN.R-project.org/package=patchwork>.
55. FC, M., Davis, T. L. & ggplot2 authors. *ggpattern: 'ggplot2' Pattern Geoms* R package version 1.0.1 (2022). <https://CRAN.R-project.org/package=ggpattern>.
56. Wickham, H. et al. Welcome to the tidyverse. *Journal of Open Source Software* **4**, 1686. doi:10.21105/joss.01686 (2019).
57. Kassambara, A. *rstatix: Pipe-Friendly Framework for Basic Statistical Tests* R package version 0.7.2 (2023). <https://CRAN.R-project.org/package=rstatix>.
58. Mauricio Zambrano-Bigiarini. *hydroGOF: Goodness-of-fit functions for comparison of simulated and observed hydrological time series* R package version 0.4-0 (2020). doi:10.5281/zenodo.839854. <https://github.com/hzambran/hydroGOF>.
59. Soil Chemistry Laboratory (CBLB). *Determination of Selected Elements in Soil after Digestion with Aqua Regia, Using ICP-OES or ICP-MS, Information Sheet* 2020. (2024).
60. Gražulis, S., Merkys, A. & Vaitkus, A. in *Handbook of Materials Modeling: Methods: Theory and Modeling* (eds Andreoni, W. & Yip, S.) 1863–1881 (Springer International Publishing, Cham, 2020). doi:10.1007/978-3-319-44677-6\_66. (2024).
61. Xu, Z., Cai, J.-g. & Pan, B.-c. Mathematically Modeling Fixed-Bed Adsorption in Aqueous Systems. *Journal of Zhejiang University SCIENCE A* **14**, 155–176. doi:10.1631/jzus.A1300029 (2013).
62. Chu, K. H. Breakthrough Curve Analysis by Simplistic Models of Fixed Bed Adsorption: In Defense of the Century-Old Bohart-Adams Model. *Chemical Engineering Journal* **380**, 122513. doi:10.1016/j.cej.2019.122513 (2020).
63. Pugliese, L. et al. Long-Term Phosphorus Removal by Ca and Fe-rich Drainage Filter Materials under Variable Flow and Inlet Concentrations. *Water Research* **247**, 120792. doi:10.1016/j.watres.2023.120792 (2023).
64. Paludan, C. & Jensen, H. S. Sequential Extraction of Phosphorus in Freshwater Wetland and Lake Sediment: Significance of Humic Acids. *Wetlands* **15**, 365–373. doi:10.1007/BF03160891 (1995).
65. Laskar, I. B. et al. Waste Snail Shell Derived Heterogeneous Catalyst for Biodiesel Production by the Transesterification of Soybean Oil. *RSC Advances* **8**, 20131–20142. doi:10.1039/C8RA02397B (2018).
66. Zhao, J. et al. Organics Wastewater Degradation by a Mesoporous Chromium-Functionalized  $\gamma$ -Al<sub>2</sub>O<sub>3</sub> with H<sub>2</sub>O<sub>2</sub> Assistance. *Water, Air, & Soil Pollution* **229**, 135. doi:10.1007/s11270-018-3789-y (2018).

67. Ogata, F., Tominaga, H., Kangawa, M., Inoue, K. & Kawasaki, N. Characteristics of Granular Boehmite and Its Ability to Adsorb Phosphate from Aqueous Solution. *Chemical and Pharmaceutical Bulletin* **60**, 985–988. doi:10.1248/cpb.c12-00211 (2012).
68. Ogata, F. et al. Granulation of Boehmite without a Binder and Its Capacity for Phosphate Adsorption in Aqueous Solution. *Journal of Water and Environment Technology* **11**, 225–234. doi:10.2965/jwet.2013.225 (2013).
69. Li, M., Liu, J., Xu, Y. & Qian, G. Phosphate Adsorption on Metal Oxides and Metal Hydroxides: A Comparative Review. *Environmental Reviews* **24**, 319–332. doi:10.1139/er-2015-0080 (2016).
70. Bleam, W. F., Pfeffer, P. E., Goldberg, S., Taylor, R. W. & Dudley, R. A Phosphorus-31 Solid-State Nuclear Magnetic Resonance Study of Phosphate Adsorption at the Boehmite/Aqueous Solution Interface. *Langmuir* **7**, 1702–1712. doi:10.1021/1a00056a023 (1991).
71. Katircioglu-Bayel, D. Optimization of Operating Parameters on Dry Grinding of Calcite in a Stirred Media Mill Using the Box-Behnken Design. *Minerals* **10**, 251. doi:10.3390/min10030251 (2020).
72. Ferraz, E., Gamelas, J. A. F., Coroado, J., Monteiro, C. & Rocha, F. Recycling Waste Seashells to Produce Calcitic Lime: Characterization and Wet Slaking Reactivity. *Waste and Biomass Valorization* **10**, 2397–2414. doi:10.1007/s12649-018-0232-y (2019).
73. Wilson, S. The Dehydration of Boehmite,  $\gamma$ -AlOOH, to  $\gamma$ -Al<sub>2</sub>O<sub>3</sub>. *Journal of Solid State Chemistry* **30**, 247–255. doi:10.1016/0022-4596(79)90106-3. (2024) (1979).
74. Shkatulov, A. I., Kim, S. T., Miura, H., Kato, Y. & Aristov, Y. I. Adapting the MgO-CO<sub>2</sub> Working Pair for Thermochemical Energy Storage by Doping with Salts. *Energy Conversion and Management* **185**, 473–481. doi:10.1016/j.enconman.2019.01.056 (2019).
75. Nadagouda, M. US20210130251A1. <https://patents.google.com/patent/US20210130251A1/en> (2023)(2021).
76. Borggaard, O., Raben-Lange, B., Gimsing, A. & Strobel, B. Influence of Humic Substances on Phosphate Adsorption by Aluminium and Iron Oxides. *Geoderma* **127**, 270–279. doi:10.1016/j.geoderma.2004.12.011 (2005).
77. Qian, J. et al. Co-Adsorption of Perfluorooctane Sulfonate and Phosphate on Boehmite: Influence of Temperature, Phosphate Initial Concentration and pH. *Ecotoxicology and Environmental Safety* **137**, 71–77. doi:10.1016/j.ecoenv.2016.11.026 (2017).
78. Hsu, P. H. in *SSSA Book Series* (eds Dixon, J. B. & Weed, S. B.) 331–378 (Soil Science Society of America, Madison, WI, USA, 2018). doi:10.2136/sssabookser1.2ed.c7.
79. Xu, N. et al. Retention of Phosphorus on Calcite and Dolomite: Speciation and Modeling. *RSC Advances* **4**, 35205–35214. doi:10.1039/C4RA05461J (2014).
80. Flower, H. et al. Why Is Calcite a Strong Phosphorus Sink in Freshwater? Investigating the Adsorption Mechanism Using Batch Experiments and Surface Complexation Modeling. *Chemosphere* **286**, 131596. doi:10.1016/j.chemosphere.2021.131596 (2022).
81. Silva, M. & Baltrusaitis, J. A Review of Phosphate Adsorption on Mg-containing Materials: Kinetics, Equilibrium, and Mechanistic Insights. *Environmental Science: Water Research & Technology* **6**, 3178–3194. doi:10.1039/D0EW00679C (2020).
82. Ekamparam, A. S. S. & Singh, A. Transformation of Calcite to Fluorapatite at Room Temperature: Impact of Initial Phosphate and Fluoride Levels. *Geochimica et Cosmochimica Acta* **288**, 16–35. doi:10.1016/j.gca.2020.07.039 (2020).
83. Wan, B. et al. Surface Adsorption and Precipitation of Inositol Hexakisphosphate on Calcite: A Comparison with Orthophosphate. *Chemical Geology* **421**, 103–111. doi:10.1016/j.chemgeo.2015.12.004 (2016).
84. Tamimi, F. et al. Biocompatibility of Magnesium Phosphate Minerals and Their Stability under Physiological Conditions. *Acta Biomaterialia* **7**, 2678–2685. doi:10.1016/j.actbio.2011.02.007 (2011).
85. Koopmans, G. F., Chardon, W. J. & van der Salm, C. Disturbance of Water-Extractable Phosphorus Determination by Colloidal Particles in a Heavy Clay Soil from the Netherlands. *Journal of Environmental Quality* **34**, 1446–1450. doi:10.2134/jeq2005.0028 (2005).
86. Jarvie, H. P., Withers, J. A. & Neal, C. Review of Robust Measurement of Phosphorus in River Water: Sampling, Storage, Fractionation and Sensitivity. *Hydrology and Earth System Sciences* **6**, 113–131. doi:10.5194/hess-6-113-2002 (2002).
87. Raupach, M. R. Solubility of Simple Aluminium Compounds Expected in Soils. I. Hydroxides and Oxyhydroxides. *Soil Research* **1**, 28–35. doi:10.1071/sr9630028 (1963).
88. Kralj, D. & Brečević, L. Dissolution Kinetics and Solubility of Calcium Carbonate Monohydrate. *Colloids and Surfaces A: Physicochemical and Engineering Aspects* **96**, 287–293. doi:10.1016/0927-7757(94)03063-6 (1995).
89. Bilotta, G. S. & Brazier, R. E. Understanding the Influence of Suspended Solids on Water Quality and Aquatic Biota. *Water Research* **42**, 2849–2861. doi:10.1016/j.watres.2008.03.018 (2008).
90. Jaishankar, M., Tseten, T., Anbalagan, N., Mathew, B. B. & Beeregowda, K. N. Toxicity, Mechanism and Health Effects of Some Heavy Metals. *Interdisciplinary Toxicology* **7**, 60–72. doi:10.2478/intox-2014-0009 (2014).
91. DeForest, D. K. et al. Updated Multiple Linear Regression Models for Predicting Chronic Aluminum Toxicity to Freshwater Aquatic Organisms and Developing Water Quality Guidelines. *Environmental Toxicology and Chemistry* **39**, 1724–1736. doi:10.1002/etc.4796 (2020).
92. Gensemer, R. W. & Playle, R. C. The Bioavailability and Toxicity of Aluminum in Aquatic Environments. *Critical Reviews in Environmental Science and Technology* **29**, 315–450. doi:10.1080/10643389991259245 (1999).
93. Lado, L. R., Hengl, T. & Reuter, H. I. Heavy Metals in European Soils: A Geostatistical Analysis of the FOREGS Geochemical Database. *Geoderma* **148**, 189–199. doi:10.1016/j.geoderma.2008.09.020 (2008).
94. Tóth, G., Hermann, T., Szatmári, G. & Pásztor, L. Maps of Heavy Metals in the Soils of the European Union and Proposed Priority Areas for Detailed Assessment. *Science of The Total Environment* **565**, 1054–1062. doi:10.1016/j.scitotenv.2016.05.115 (2016).
95. Zhu, L.-k. et al. Studies on Fluid Dynamics of the Flow Field and Gas Transfer in Orbitally Shaken Tubes. *Biotechnology Progress* **33**, 192–200. doi:10.1002/btpr.2375 (2017).
96. Rozemeijer, J. C. et al. Integrated Modeling of Groundwater–Surface Water Interactions in a Tile-Drained Agricultural Field: The Importance of Directly Measured Flow Route Contributions. *Water Resources Research* **46**. doi:10.1029/2010WR009155 (2010).

## Appendix A Supplementary protocols

### A.1 Product interference with the SFA

Any given sample must be filtered when measuring the soluble reactive phosphorus (SRP). The simplest would be to use a syringe fitted with a 0.45  $\mu\text{m}$  membrane filter cartridge. Still, colloidal material may still seep through (SFA) (Skalar, SAN+ System). A simple test was done to determine whether this was the case.

2 g of Eutrosorb® F and Phosflow™ was weighed and transferred into separate 50-mL centrifuge tubes, to which 40 mL deionised water (DIW) was added. Similarly, blanks without either product were prepared. These tubes were all shaken for 27 h at around 100 RPM. Once incubated, 30 mL was taken from each tube, half of which was filtered using a 0.45  $\mu\text{m}$  membrane filter cartridge. These two fractions were then split once more, and to one half, 86  $\mu\text{L}$  8 mg P L<sup>-1</sup> was added. Thus, there were 12 treatments: samples with Eutrosorb® F, Phosflow™, or no product; filtered and unfiltered samples; samples with added P and those without. Every treatment was prepared in quintuplet. All samples were stored at -20 °C until analysis. The filtered samples were analysed for SRP and the unfiltered ones for total P using the SFA at 880 nm. The treatments with added P were corrected for background P, using the average of the measured P in the blank samples without added P.

In order to find out whether the products reduce the signal compared to the blank with added P, the product treatments with added P were compared to the blanks with added P using the Wilcoxon signed-rank test. Similarly, to find out the opposite, the same test was used to compare the product treatments without added P with the blank treatments without added P.

The results are shown in Figure A.1. The implication from this figure is that in unfiltered samples, Phosflow tends to add a background to the signal when measuring at higher sensitivities. Both lead to some background when measuring using unfiltered samples at lower sensitivities. However, when P is added, Eutrosorb F lowers the signal at the higher sensitivity, whereas Phosflow increases the signal at lower sensitivity. One conclusion that may be drawn, is that some product in colloidal form is passed through the filters that were used, leading to distortions to the signal. Thus, as a preventative measure, samples for SRP analysis after the kinetics experiment were filtered using 0.2  $\mu\text{m}$  membrane filters, i.e., filters with smaller pores.

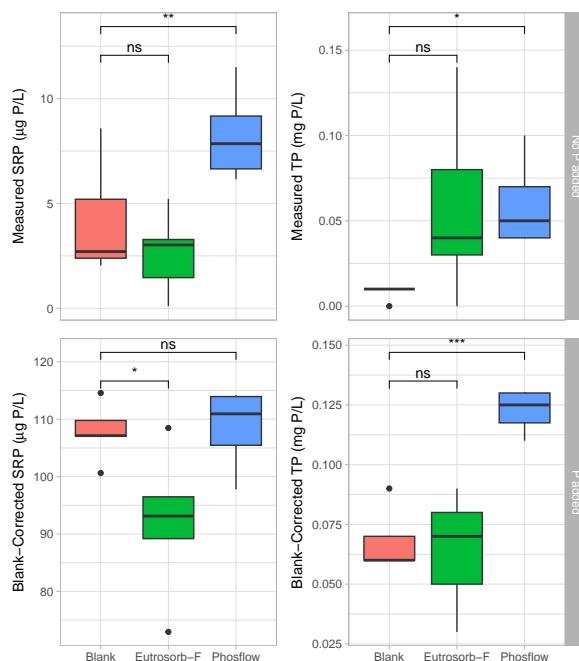


**Figure A.1 – Product interference in the SFA** – Comparison of the different treatments for testing the product interference in the SFA. Significance symbols are the same as elsewhere.

## A.2 Sequential P-extraction; in-house protocol

The protocol in Figure A.2 and Figure A.3 was carried out exactly, with some notable deviations. i) Instead of performing 2 separate extractions in phase 1, 1 extraction with 50 mL oxygen-free distilled water was done. ii) The second extraction in phase 2 was performed over 30 instead of 5 min. iii) The washes with distilled water in the third and fourth phase were performed over 30 instead of 5 min. iv) In phase 4, 2 HCl extractions were done instead of 1. The first 3 deviations were the result of practical considerations. The fourth was done because it was feared that the pH-buffering capacities of the products (see also Figure 6 and Figure B.2 b)) would neutralise the acid too much. This would lead to an underestimation of this fraction and an overestimation of the fraction of phase 5.

### P0803 Sequential P fractionation sediments

Date: modified 2015/2019 (ML/MM) Update: dec 2022 (WB)

Reference: Modified by Miquel Lurling from Paludan & Jensen 1995, Wetlands 15 365-373 Sequential Extraction of Phosphorus in Freshwater Wetland and Lake sediment: significance of Humic Acids.

**Materials:**

- 50 ml centrifuge tubes
- dispenser 25 mL
- Eppendorf pipettes/tips
- shaker
- centrifuge
- air-flush installation
- glass Pasteur pipets
- PE bottles 50 and 100mL
- filtration device and GF/C filters
- crucibles with lid and tongs
- drying Oven
- Furnace/ignition oven 550 °C/hot-plate (120°C)

**Chemicals:**

**Oxygen-free nanopure water**  
bubble Milli-Q water 15 minutes with N<sub>2</sub>

**BD-reagent** : 0.11 M Na<sub>2</sub>S<sub>2</sub>O<sub>4</sub> / 0.11 M NaHCO<sub>3</sub>  
(38 g Na<sub>2</sub>S<sub>2</sub>O<sub>4</sub>/2L + 18,4 g NaHCO<sub>3</sub>/2L)

**0.1 M NaOH-solution**  
(8,0 g NaOH/2L)

**0.5 M HCL-solution**  
(83,3 mL HCl-37%/2L)

**2M H<sub>2</sub>SO<sub>4</sub>**  
(54.5 mL H<sub>2</sub>SO<sub>4</sub>- 95-97%/500mL)

Sediments collected from field **Keep collected sediments frozen upon analysis**

**Method**  
See: Schematic overview of sequential P fractionation of sediment

**Shaking**  
use shaker ~140 rpm  
Shake tubes horizontally

**Centrifugation**  
5 minutes at 5000 rpm

**Decant carefully**  
don't let the silt slip out pellet sample

**Filtration**  
1,2 µm (GF/C)filter, vacuum filtration

**Bubbling N<sub>2</sub> / aeration**  
Please ask technician

➤ **Analysis**

1. Tvan (sived) sediments and mix thoroughly
2. Take 50 mL centrifuge tubes with cap. Weigh in 1.0 g of sediment to each tube

➤ **First phase:** Oxygen-free nanopure water -->It aims to release the available P, which is the interstitial water loosely adsorbed to surfaces of Fe and CaCO<sub>3</sub>

1. add 25 mL of oxygen-free nanopure water. Replace air with N<sub>2</sub> and close tube.
2. Shake tubes for 30 minutes.
3. Place the tubes in centrifuge, centrifuge
4. Decant supernatant **carefully** into labelled 100mL PE bottle, save pellet
5. Repeat extraction with 25 mL oxygen-free water for 5 minutes and centrifuge.
6. Decant and combine supernatant.
7. Filter the supernatant over a GF/C filter and collect 30 mL filtrate in a labelled 50 mL PE bottle.

Store this fraction in freezer immediately

Measure PO<sub>4</sub>-P

➤ **Second Phase:** BD-reagent (bicarbonate-dithionite mixture) -->aim: stronger reductant that will release the SRP bound manly to Fe-hydroxides and Mn-compounds

1. Add 25 mL BD-reagent, oxygen-free, to sediment pellet (from previously phase). Replace air with N<sub>2</sub> and close tube.
2. Shake tubes for 30 minutes.
3. centrifuge
4. Decant supernatant into 100 mL PE bottles.
5. Add 25 mL BD to pellet, replace air with N<sub>2</sub>.
6. Shake tubes on shaker for 5 minutes,
7. centrifuge
8. decant and combine supernatant. Save pellet
9. Put sample bottles in Aeration-set-up
10. Aerate for 30 minutes  
(removal dithionite; keeps Fe and PO<sub>4</sub> in solution)



The fumes that are released during this process must be extracted, install aeration-set-up in fume hood

Figure A.2 – Sequential P-extraction; page 1 – Page 1 of the in-house protocol for sequential P-extraction.

10. Add 3 mL 2M H<sub>2</sub>SO<sub>4</sub> to the combined supernatants and mix.  
 11. Filter combined supernatants, collect 30 mL filtrate into 50 mL PE bottle. Label well and store at 4 °C

Measure PO<sub>4</sub>-P and TP (total fraction of the dissolved)

➤ **Third Phase: Sodium Hydroxide (NaOH)** --> It will extract SRP sorbed by clay- and metal-oxides (Al)

1. Add 25 mL 0,1 M NaOH to the sediment pellet and close tube.
2. Shake tubes 30 minutes on shaker.
3. centrifuge
4. Decant supernatant into 100 mL PE bottle.
5. Add 25 mL NaOH to sediment pellet.
6. Shake again 30 minutes on shaker and centrifuge.
7. Combine supernatants into 100 mL PE bottle.
8. Add 25 mL of **milli-Q water** to the sediment and shake for 5 minutes, centrifuge
9. Decant the third supernatant in the same 100 mL PE bottle. Save pellet
10. Add 1.5 mL of 2M H<sub>2</sub>SO<sub>4</sub> in the supernatant and mix.
11. Filter the supernatant and collect 30 mL filtrate into 50 mL bottle

Measure PO<sub>4</sub>-P and TP (total fraction of the dissolved)

➤ **Fourth Phase: Hydrochloric acid** --> Aim to release P bound to carbonates and apatite-P. This is hardly bioavailable

1. Add 25 mL 0,5 M HCl and close tube. Shake for 1 hour
2. Centrifuge
3. Decant supernatant into 100 mL PE bottle
4. Add 25 mL Milli-Q water to the sediment, shake for 5 minutes.
5. centrifuge
6. Combine supernatants and filter through GF/C. collect 30 mL filtrate and store at 4 °C.
7. Save pellet

Measure PO<sub>4</sub>-P and TP (total fraction of the dissolved)

➤ **Fifth Phase: Finally, the sediment pellet will be extracted using stronger acid and higher temperature. This will give the refractory P**

1. Move the pellet to crucibles use little milli-Q water
2. Dry crucibles at 105 °C in drying oven, over-night
3. Ignite pellet at 550 °C for 2 hours
4. Cool down and "crumble" pellet in crucible
5. Add 10 mL 2M H<sub>2</sub>SO<sub>4</sub> and mix
6. Place crucibles with lid on hot-plate (in fume hood) and boil 10 minutes at 120 °C
7. Take-up sample by 10 mL syringe, add filter-disc.
8. Filter sample in a labelled 15 mL tube

Measure PO<sub>4</sub>-P

➤ **Also conduct digestion on dry sediment to determine the total-TP, see protocol: P0802** determination of total N&P in sediments

➤ **Determine the moisture content of the sediments used, see protocol: P0602** Dry matter and moisture content of sediments

**Calculation**

Calculate P in each fraction using results Phase 1 -5

$$[P_{sed}] = \frac{[P_f] \times V_{extract}}{DW}$$

In which  $P_{sed}$  = [P] in sediment (µg P g<sup>-1</sup> DW),  $P_f$  = [P] in fraction (µg P mL<sup>-1</sup>),  $V_{extract}$  = volume extractant (mL),  $DW$  = dry-weight sediment (g).

Figure A.3 – Sequential P-extraction; page 2 – Page 2 of the in-house protocol for sequential P-extraction.

### A.3 Estimation of flow velocity in shaking test

During the shaking experiment, the mixtures sat in a 50-mL tube. Assuming that the 40 mL was transported entirely side-to-side. With  $100^{-1} \text{ min rnd}^{-1}$  and a back-and-forth 'discharge' of  $20 \text{ mL rnd}^{-1}$ , the material experienced  $20/100 = 2 \text{ L min}^{-1}$ . For 140 RPM, this would be  $2.8 \text{ L min}^{-1}$ . Given the cross-section of  $5.73 \text{ cm}^2$ , the maximum average flow velocities would be  $5.8$  and  $8.2 \text{ cm s}^{-1}$  respectively. These estimates are somewhat larger than the axial velocities in the work by Zhu *et al.* [95] on flow in vertically rotated 50-mL disposable bioreactors, but they are of similar order of magnitude. Thus, the actual average flow velocities may be between the found values, and some smaller values.

## Appendix B Supplementary results and measurements

This appendix contains results supplementary to those in section 3. Table B.1 shows the measured blanks during the shaking test. Figure B.1 shows the measured flow rates, dissolved oxygen, and lakewater total nitrogen (TN) for the fixed-bed experiment. Figure B.2 gives the soluble reactive P (SRP) and  $Q$  timeseries for all bottles in the kinetics experiment, along with the average pH and measured temperatures. Table B.2 shows the models for all bottles with product in the kinetics experiment. Table B.3 shows the attributes measured for the products that were loaded with P; dry weight, mass loss, SRP, and  $Q$  are all given. Table B.5 gives the found breakthrough curve parameters. Table B.4 shows the modelling results of the shaking test in greater detail, giving the model coefficients for all modelled variables. Table B.5 gives the fixed-bed model parameters, both the linear parameters and the calculated Bohart-Adams parameters. Table B.6 gives  $Q_{total}$  for the products used in the sequential P extraction. Figure B.4 gives the  $Q$  for all pools across the products with standard deviations in the sequential P extraction. Figure B.5 gives the relative distribution of the loaded products in the sequential P extraction. Table B.7 gives a pair-wise comparisons of the measured concentrations in the sequential P extractions, where similar letters indicate homogeneous groupings that cannot be differentiated at the 95% level.

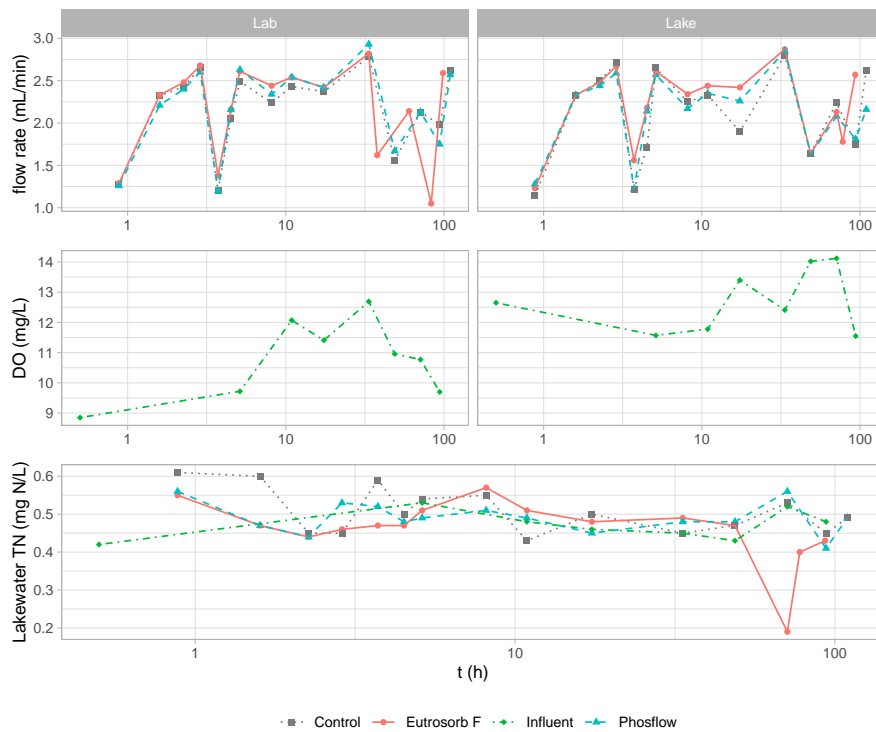


**Figure B.1 – Fixed-bed adsorption; other endpoints** – Shown are: flowrates as determined through all outlets in the fixed-bed adsorption experiment; dissolved oxygen in the influent; and total nitrogen in all the lakewater samples

**Table B.1 – Shaking test; blanks** – Shown are the measured pH and EC of the blanks for various shaking regimes. In practice, then, these are from 40-mL DIW in 50-mL centrifuge tubes in equilibrium with the overhead space. The gases of the initial overhead gas should have the same composition as the laboratory. The strategy of the blanks was poorly thought out, as can be seen from this table. No linear trends were visible per blank series over time ( $R^2 < 0.3$ ). The EC were not normally distributed (Shapiro-Wilks,  $p < 0.05$ ), hence the median is given.

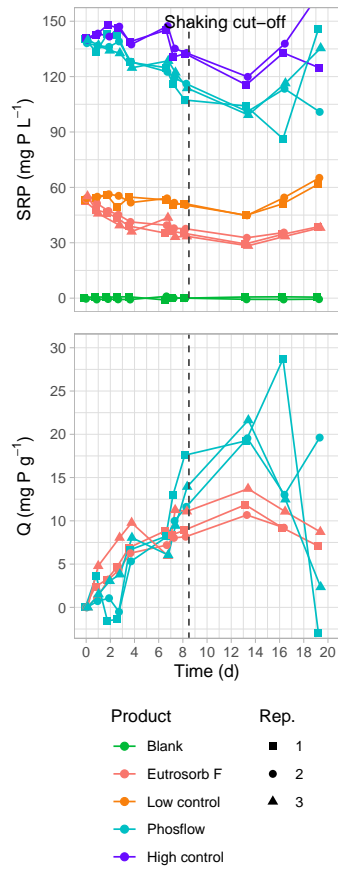
Shake	Time (d)	pH (-)	EC ( $\mu\text{S cm}^{-1}$ )
Still	1	-	0.6
		-	0.6
		-	0.9
	3	5.48	14.6
		6.37	5.6
		6.08	2.6
7	6.092	6.9	
Weak	3	5.84	7
		5.15	2
	7	5.41	5
		5.12	4
Strong	1	5.775	2.4
		5.479	3.5
mean		5.6796	
$\sigma_{\text{pH}}$		0.420088	
median			3.5

**Table B.2 – Adsorption kinetics; all models** – The experimental time series from every bottle, both SRP and  $Q$ .

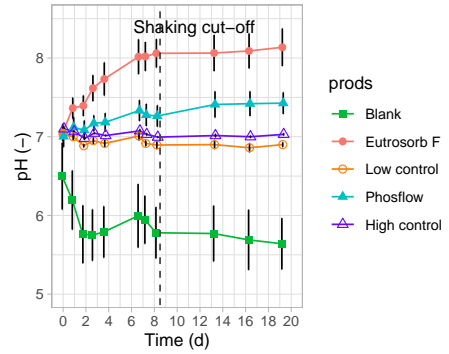
Time series	$Q_{\text{max}}$	$k$ ( $\text{d}^{-1}$ )	$R^2$	
EutroSORB®F	1	9.53	0.305	0.89
	2	10.2	0.210	0.97
	3	10.5	0.582	0.76
Phosflow™	1	16.0	0.163	0.36
	2	31.6	0.0482	0.89
	3	12.0	0.237	0.47

**Table B.3 – XRD; adsorbed P-content in loaded samples** – SRP measured and  $Q$  calculated after incubating the material meant for XRD analysis. The mass loss after incubation and drying  $\Delta M$  is also given as a percentage of the wet weight. The error given on the initial concentration of the solution is the standard deviation ( $N = 2$ )

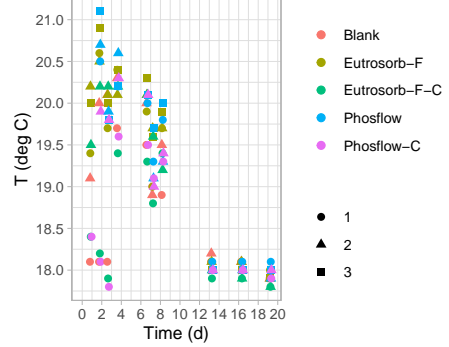
Product	DW (g)	$\Delta M$ (%)	SRP ( $\text{mg P L}^{-1}$ )	$Q$ ( $\text{mg P g}^{-1}$ DW)
Initial	-	-	100 ( $\pm 5$ )	-
EutroSORB® F	18.54	7.7	57	4.64
Phosflow™	9.95	0.38	77	4.62



a) SRP and Q – SRP and the calculated Q over time.



b) pH – The average pH measured in the bottles at every time step.



c) Temperatures – The average temperatures measured in the bottles at every time step.

**Figure B.2 – Adsorption kinetics; all experimental time series** – The experimental time series from every bottle: SRP and the calculated Q in Figure B.2 a); pH over time Figure B.2 b); temperature over time Figure B.2 c).

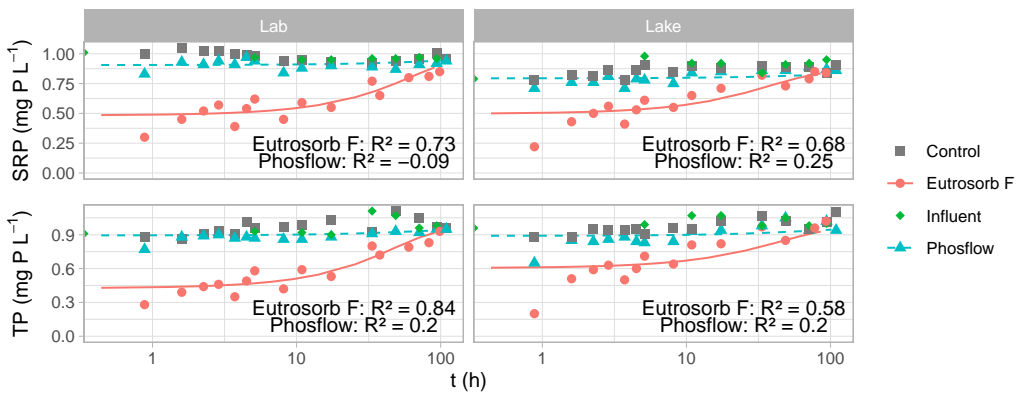


**Figure B.3 – Fixed-bed adsorption; breakthrough curves** – The SRP and TP measured across the various beds. The drawn trends are fitted breakthrough curves according to Equation 9.

**Table B.4 – Product response to physical agitation in water; Linear regression results** – The results of the multilinear regression of the data gathered in the experiment determining the response to mechanical agitation. For a given product, the linear regression coefficients are given for the models of every quantity which was modelled. The number underneath every coefficient is the standard error associated with the respective coefficient. Furthermore, the signs, ‘, ‘\*, ‘\*\*, and ‘\*\*\* indicate that for the indicated coefficient or model of a quantity, the associated p-value was < 0.1, 0.05, 0.01, or 0.001, respectively. Finally, the F-statistic and adjusted  $R^2$  are given for every model. Empty rows indicate that no significant model was found.

Product	Quantity	$R^2$	Intercept	$t_{\text{shake}}$	Still	Weak	Strong	$t_{\text{shake}}:\text{Still}$	$t_{\text{shake}}:\text{Weak}$	$t_{\text{shake}}:\text{Strong}$
Phosflow	pH**	0.315	9.95***					-0.019	0.31	0.039*
	EC***	0.977	0.06	14.8***	164***	132***	137***	0.017	0.17	0.17
	$\Delta M_{\text{shake}}$ ***	0.97		1.3	6	8	8		-6.6**	1.8
	$\Delta M_{\text{SS}}$ ***	0.976			-0.85	0.52	4.1**	0.10	0.039	3.22***
EuroSORB F	pH***	0.582		-0.020**	9.08***	-0.097*	-0.19***			
	EC*	0.379		0.006	0.04	0.04	0.04			
	$\Delta M_{\text{shake}}$			4.5**	178**	27**	17			
	$\Delta M_{\text{SS}}$ ***	0.878	2.4***	1.5	9	9	9			
			0.5					-0.17	-0.17	1.30***
								0.12	0.12	0.12

**Table B.5 – Fixed-bed adsorption; modelling results** – The coefficient of the linear model regression of the fixed-bed time series, and derived coefficients for the Bohart-Adams model. The number below the first gives the standard error on the number above, with errors of the Bohart-Adams coefficients being derived from linear standard error propagation. The following errors were assumed:  $\sigma_M = 0.001$  g,  $\sigma_{C_F} = 0.02$  mg P L<sup>-1</sup>, and  $\sigma_q = 0.145$  mL min<sup>-1</sup>. Significance of coefficients is given, with ‘\*\*\*’, ‘\*\*’, ‘\*’, and ‘.’ being symbols for  $p < 0.001$ ,  $p < 0.01$ ,  $p < 0.05$ , and  $p < 0.1$  respectively.

Model	Coefficient	EuroSORB F			Phosflow			
		Lab	TP	SRP	Lab	TP	SRP	
Linear	$b$ (-)	0.25	2.35	-3.15	-5.07	-25.3***	-25.5***	-24.3***
	$m$ (week <sup>-1</sup> )	1.6	1.7	2.4	2.4	2.2	4	1.5
	$R^2$	4.22***	5.97***	6.35***	5.12**	1.28	1.94	1.36
Bohart-Adams	$k_B$ (L mg <sup>-1</sup> week <sup>-1</sup> )	0.8	0.8	1.2	1.3	1	1.5	0.7
	$Q_{\text{max}}$ (mg P g <sup>-1</sup> )	0.69	0.8	0.69	0.57	0.06	0.06	0.22
		4.3	6.1	7.4	6.0	1.3	2.0	1.6
		0.8	0.9	1.4	1.5	1	1.5	0.8
		4.8	3.9	2.2	2.3	2.6	1.7	2.1
		1.1	0.8	0.6	0.8	2	1.4	1.1

**Table B.6 – Sequential P extraction; total Q** – Total  $Q$  ( $\text{mg P g}^{-1}$ ) found after sequential P extraction of the products. The errors are standard deviations ( $N = 3$ ).

Series	Phosflow™	Phosflow™, loaded	EutroSORB®F	EutroSORB®F, loaded
Mean	0.01 $\pm$ 0.06	5.49 $\pm$ 0.5	0.01 $\pm$ 0.04	5.64 $\pm$ 1.7
1	0.00	5.57	0.00	5.47
2	0.04	5.28	0.03	5.07
3	0.01	5.63	0.00	6.39

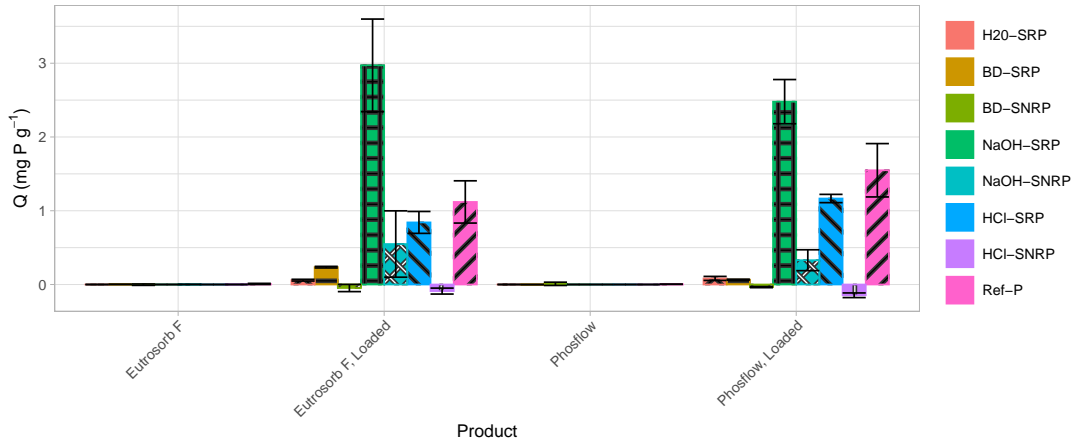


**Figure B.4 – Sequential P extraction; separate pools with errors** – The absolute  $Q$  found for all products. The indicated errors are standard errors ( $N = 3$ ).

### Estimating product lifetimes

Given Equation 11 and Equation 10, back-of-the-envelope estimations of product-lifetime under more realistic conditions were done. For this, low-flow conditions in drainage pipes similar to that found in Rozemeijer *et al.* [96] were taken, around  $2 \text{ L min}^{-1}$  as well as  $0.2 \text{ L min}^{-1}$ . Furthermore, it was assumed that field application would involve around  $2 \text{ kg product}$ . Matching other filter-material investigations in Mendes *et al.* [39],  $C_0$  was taken to be  $0.5 \text{ mg P L}^{-1}$ . Then, using  $CC_0^{-1} = 0.5$  and  $CC_0^{-1} = 0.95$ , corresponding  $t_{\text{life}}$  were calculated by solving Equation 9 for  $t$  with the aforementioned numbers plugged in and  $Q_{\text{max}}$  and  $k_B$  as found for the SRP-based models.

Estimated  $t_{1/2}$  (lifetimes for which  $CC_0^{-1} = 0.5$ ) for Phosflow™ were negative in the Baseflow scenarios ( $2 \text{ L min}^{-1}$ ) (Figure B.6). This indicates that removal would already be well below 50% at the beginning of application. For EutroSORB® F, these times are between 5 and 10 d. During low flow ( $0.2 \text{ L min}^{-1}$ ), both products perform much better, between 30 and 40 d for Phosflow™. EutroSORB® F hangs around for around 75 days in lab-based water, and around 35 days in lake-water-based influent. The large differences between  $CC_0^{-1} = 0.5$  and  $CC_0^{-1} = 0.95$  values for Phosflow™ indicate rather shallow breakthrough curves, whereas those of EutroSORB® F imply much steeper curves.

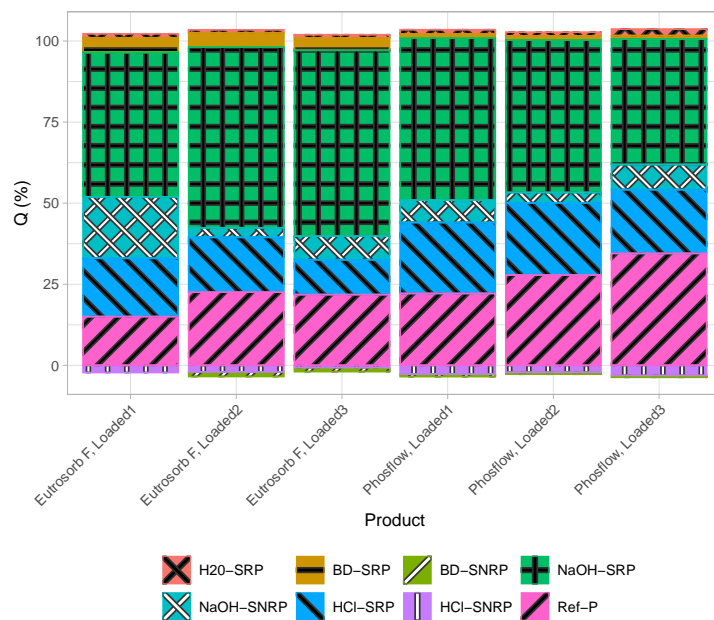


**Figure B.5 – Sequential P extraction; relative pools loaded products –** Relative P pools of every loaded extraction.

**Table B.7 – Sequential P extraction; Comparisons –** Significantly different groups of products for every fraction when comparing C ( $\text{mg P L}^{-1}$ ) across products. Thus, each row is one comparison: kruskal-wallis followed by Dunn's test with  $\alpha = 0.05$ . Similar letters indicate homogeneous groupings that cannot be differentiated at the 95% level.

Fractions	Blank	EutroSORB® F Empty	Loaded	Phosflow™ Empty	Loaded
H2O	a	a	b	a	b
BD SRP	ab	ab	c	a	bc
BD SNRP	a	a	b	a	ab
NaOH SRP	a	ab	c	a	bc
NaOH SNRP	a	a	b	ac	bc
HCl SRP	a	ab	bc	a	c
HCl SNRP	a	ab	bc	a	c
H2SO4	a	ab	bc	ab	c

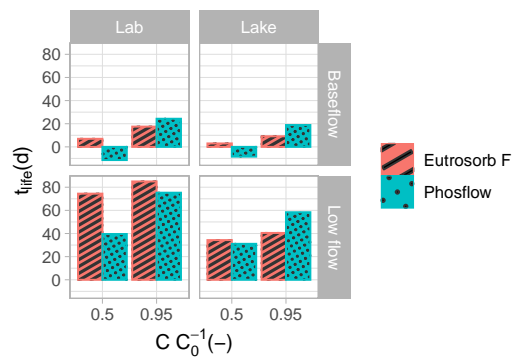


**Figure B.6 – Fixed-bed adsorption; estimated lifetimes** – Product lifetimes inferred from SRP-based model parameters and more realistic environmental conditions for 2 kg product. Here,  $C_0 = 0.5 \text{ mg P L}^{-1}$ , 'Baseflow' refers to  $q = 2 \text{ L min}^{-1}$ , and 'Low flow' refers to  $q = 0.2 \text{ L min}^{-1}$ .

## Appendix C Personal Communications and Declarations

### C.1 Summary of the meeting on June 10, 2023

*Here follows a summary of the meeting held on June 10, 2023, at 13:00 UTC, regarding the filter media and relevant topics for this report. Present were J.C. (Johan) van Snippenberg, the author of this proposal; my supervisors, M.F.L.L.W. (Mike) Lüring and M.N.T. (Maíra) Mucci; B.C. (Byran) Fuhrmann and K.E. (Kate) Waters-Hart from EutroPHIX and Phoslock Environmental Technologies (PET) respectively.*

The patent we found for the phosflow is probably from another product, because there is no lanthanum in there, as noted by Kate. Instead, there is aluminium oxide and magnesium carbonate in there. The product that we found is the one supposed to be used in wastewater treatment, whereas phosflow is meant for stormwater treatment. Mike notes that there are confusing data on the phosflow website, especially the timelines, which turns out are constructed based on experiments on different conditions: i.e., two result from lab tests and two are from field trials. (Kate), the folks from Australia have not really given here the data that she would like to have.

Mike noted that filtered lake water can be used in some of the experiments.

The products are used in small plastic mesh bags. However, phosflow is also intended to be used in cages and anything else that can keep them in one place [Kate]. As such, it would be a good idea to work them into the methods somehow. Specifically, the ones where I look at the stability of the things, and where they are shaken for longer periods of time.

According to Byran, upscaling of the products is a real problem. In small amounts, it is clear that [Eutrosorb F] has a very nice adsorption capacity. However, when put together in larger quantities, the adsorption is much poorer: the bags can really restrict flow, thereby reducing discharge through the bag and hence removal efficiency. They [Byran] did tests in which they put the materials at the end of drainage pipes, where water was sure to be forced through the material: very high removal was achieved then. The materials work best when water can be forced through them.

For identifying what the material is, Byran suggested acid digestion and then using ICP-MS. Check for elements like Fe, Mg, Al, Ca, La, etc. He suggested testing the buffering capacities of the materials, that is, treating it with acid and do a titration to see how much oxyanions versus oxides are in there. I should look this up in more detail. He says that I could expect to find Al in there.

Furthermore, he warns me that Fe and Al tend to exaggerate the adsorption capacity compared to natural conditions and compared to flowing conditions. That is, the environmental conditions can substantially impair the adsorption capacity of a sorbent. Regarding the fixed-bed, go up to 1 or 2 mg/L, go down to 50 µg/L P as initial conditions.

Suggestion for another experiment: He suspects that the adsorbents, on Al basis in particular, when used in shallow lakes, can form a substrate for algae. An idea would be to make a larger batch of saturated material and see if it can be used as a growth medium in a solution with non-limiting amounts of Nitrate and Ammonium + micronutrients, and seeding it with a known algae strain. The algaemists could be used for this.

Desorption was also tested to some degree. It could be done with just a solution, but it can also be used with plants directly. Use a P-less synthetic soil, mix used product in and see what happens. Use positive control with known P-additive to soil, and negative control without any P in there. The product(s) would then fall somewhere in between.

Kate suggested I test the materials in anoxic conditions. Maíra noted that this may also be inferred from fractionation of saturated material. That is to say, once I know what is in there, I may fractionate them based on this, and see which parts of the P are adsorbed to what aspects of the material.

Byran noted that I should make rather large batches of saturated material in solution. Maíra noted that I would probably need more material than is currently available.

### C.2 Declaration on the use of generative AI

In designing experiments, analysing and interpreting results, and writing this report, no use has been made of any generative artificial intelligence.